Available online at www.sciencedirect.com
SCIENCE DIRECT®
Journal of Computational Physics 193 (2004) 708–738
JOURNAL OF COMPUTATIONAL PHYSICS
www.elsevier.com/locate/jcp

Study on gas kinetic unified algorithm for flows from rarefied transition to continuum

Zhi-Hui Li [a,b,*], Han-Xin Zhang [b]

[a] Department of Engineering Mechanics, Tsinghua University, Beijing 100084, PR China
[b] China Aerodynamics Research and Development Center, P.O. Box 211, Mianyang 621000, PR China

Received 13 September 2001; received in revised form 13 June 2003; accepted 19 August 2003

Abstract

The modified BGK equation adapted to various flow regimes can be presented by the aid of the basic characteristics on molecular movement and collision approaching to equilibrium. The discrete velocity ordinate method is developed and applied to the velocity distribution function to remove its continuous dependency on the velocity space, and then the velocity distribution function equation is cast into hyperbolic conservation law form with nonlinear source terms. Based on the unsteady time-splitting method and the non-oscillatory, containing no free parameters, and dissipative (NND) scheme, the gas kinetic finite difference second-order scheme is constructed for the computation of the discrete velocity distribution functions. The mathematical model on the interaction of molecules with solid surface is studied and used in the numerical method. Four types of numerical quadrature rules, such as the modified Gauss–Hermite formula, the composite Newton–Cotes integration method, the Gauss–Legendre numerical quadrature rule, and the Golden Section number-theoretic integral method, are developed and applied to the discretized velocity space to evaluate the macroscopic flow parameters at each point in the physical space. As a result, a unified simplified gas kinetic algorithm is established for the flows from rarefied transition to continuum regime. Based on analyzing the inner parallel degree of the unified algorithm, the parallel strategy adapted to the gas kinetic numerical algorithm is studied, and then the HPF parallel processing software for the unified algorithm is developed. To test the present method, the one-dimensional shock-tube problems, the flows past two-dimensional circular cylinder, and the flows around three-dimensional sphere and spacecraft shape with various Knudsen numbers are simulated. The computational results are found in high resolution of the flow fields and good agreement with the theoretical, DSMC, N–S, and experimental results.

Keywords: Kinetic theory of gases; Velocity distribution function; Boltzmann model equation; Discrete ordinate method; Time-splitting method; NND finite difference scheme; Rarefied gas flow; Continuum flow

* Corresponding author. Tel.: +86-10-8231-7015; fax: +86-10-8231-7341.
E-mail address: zhli0097@x263.net (Z.-H. Li).

0021-9991/$ - see front matter
doi:10.1016/j.jcp.2003.08.022

1. Introduction

Because of the complexity of the nonlinear integral-differential nature of the Boltzmann equation [1,2], mathematical difficulties are indeed formidable, which one encounters in handling the full Boltzmann equation for the analysis of the gas dynamic phenomena from various flow regimes. In order to make the problem tractable, the Monte Carlo method to simulate the Boltzmann equation has been presented [3–5] in the view of the theory of microscopic molecular dynamics. The direct simulation Monte Carlo (DSMC) method [6–8] has been widely used in the rarefied gas dynamics, in which the movement and collision between molecules are uncoupled over the discrete time interval small compared with the mean free time per molecule. While it has been greatly successful for the DSMC method to simulate the rarefied gas flows with large Knudsen numbers, it is very difficult for the DSMC method to simulate the transition or continuum flows with small Knudsen numbers due to the limitation to the cell size and time step of the method for itself. In addition, kinds of kinetic model equations resembling to the original Boltzmann equation concerning the various order of moments have been put forward [9–15] according as the mass, momentum, and energy conservation laws. Based on the zeroth, first, and second-order approximation of the Maxwellian distribution, the Euler, N–S, and Burnett equations describing the macroscopic gas dynamics can be, respectively, deduced by applying the Chapman–Enskog expansion [1] to the Boltzmann equation or the simple BGK model equation. As a simplified form of the full Boltzmann equation, the BGK model equation provides a more tractable way to solve comparatively complex gas flow problems, which [9,16,17] supposes that the effect of collisions is roughly proportional to the departure of the true velocity distribution function from a Maxwellian. However, the model predicts [18,19] that the Prandtl number is unity whereas the correct value for a monatomic gas is very nearly 2/3, in which the collision frequency is independent of velocities. It has been suggested from the [1,7,20,21] that a unified simplied velocity distribution function equation can qualitatively describe complex gas flows from various flow regimes, which is described in Section 2. Thus, as a qualitative method, instead of solving the full Boltzmann equation one solves the modified BGK equation and probably finds a unified numerical algorithm for flows over a wide range of Knudsen numbers.

Based on concepts from the kinetic theory of gases, some gas-kinetic numerical methods [22,23] have been developed to solve continuum problems from inviscid compressible gas dynamics, which use Boltzmann-like equations as the starting point. In the 1990s, applying the asymptotic expansion of the molecular velocity distribution function to the Maxwellian distribution based on the flux conservation at the cell interface, new BGK-type schemes [24–26] adapt to compressible flows of continuum regime have been presented according to the thoughts of the Chapman–Enskog expansion. The schemes have successfully simulated many of problems, such as one-dimensional shock structures, two-dimensional shock wave reflections, inviscid and viscous flows, etc. In the computation of rarefied gas flows, the high resolution explicit and implicit finite difference methods to solve two-dimensional nonlinear BGK–Boltzmann equations have been set forth [27–32] on the basis of the introduction of the reduced velocity distribution functions and the application of the discrete ordinate method. The reliability and efficiency of the method have been demonstrated in applications to both steady and unsteady one- and two-dimensional rarefied gas dynamical problems.

In this study, based on the basic characteristics of molecular movement and collision approaching to equilibrium, the modified BGK equation adapted to various flow regimes can be described. In terms of the principle of probability statistics in the kinetic theory of gases, the discrete velocity ordinate technique is developed and applied to the velocity distribution function equation in order to replace its continuous dependency on the velocity space, and then the single equation will be cast into hyperbolic conservation equations with nonlinear source terms in the physical space and time. Drawing on the decoupling technique on molecular movement and collision in the DSMC method, the unsteady time-splitting method is used to split up the discrete velocity distribution function equations into the colliding relaxation equation and the

convective movement equations. The non-oscillatory, containing no free parameters and dissipative (NND) scheme [33,34], is employed to solve the convective equations and the second-order Runge–Kutta method is used to numerically simulate the colliding relaxation equation. The gas kinetic finite difference method for directly solving the molecular velocity distribution functions will be established by the way of coupling and iteration. To improve the computational efficiency for various Mach number flows, four types of quadrature rules, such as the modified Gauss–Hermite quadrature formula [35] and the Golden Section number-theoretic integral method which is developed out of the original works [36] of Hua and Wang, are applied to the discretized velocity space to select the discrete velocity grid points and evaluate the macroscopic flow parameters at each point in the physical space. As a result, a unified simplified gas kinetic algorithm will be developed for the gas dynamical problems from various flow regimes. Based on the parallel characteristics of the respective independent discrete velocity points in the discretized velocity space, the parallel project suitable for the gas kinetic numerical algorithm is investigated, and then the HPF (High Performance Fortran) parallel program software capable of effectively simulating the gas dynamical problems covering the full spectrum of flow regimes will be developed for the unified algorithm. To illustrate the feasibility of the present algorithm, the one-dimensional shock-tube problems, the supersonic flows past circular cylinder, and the gas flows around three-dimensional sphere and spacecraft shape with various Knudsen numbers will be simulated.

2. Description of the simplified velocity distribution function equation for various flow regimes

The Boltzmann equation [1] can describe the molecular transport phenomena from full spectrum of flow regimes in the view of micromechanics and act as the basic equation to study the gas dynamical problems. It represents the relationships between the velocity distribution function which provides a statistical description of a gas at the molecular level and the variables on which it depends. The gas transport properties and the governing equations describing macroscopic gas flows can be obtained from the Boltzmann or its model equations by using the Chapman–Enskog asymptotic expansion method. Based on the investigation to the molecular colliding relaxation from Bhatnagar et al. [9], the BGK collision model equation [9,16,17] was proposed by replacing the collision integral term of the Boltzmann equation with simple colliding relaxation model,

$$\frac{\partial f}{\partial t} + \vec{V} \cdot \frac{\partial f}{\partial \vec{r}} = -v_m(f - f_{\mathrm{M}}), \tag{1}$$

where f is the molecular velocity distribution function which depends on space $\vec{r}$, molecular velocity $\vec{V}$, and time t, f_{M} is the Maxwellian equilibrium distribution function, and v_m is the proportion coefficient of the BGK equation, which is also named as the collision frequency,

$$f_{\mathrm{M}} = n/(2\pi RT)^{3/2} \exp\left[-c^2/(2RT)\right]. \tag{2}$$

Here, n and T, respectively, denote the number density and temperature of gas flow, R is the gas constant, and c represents the magnitude of the thermal (peculiar) velocity $\vec{c}$ of the molecule, that is $\vec{c} = \vec{V} - \vec{U}$ and $c^2 = c_x^2 + c_y^2 + c_z^2$. The $\vec{c}$ consists of $c_x = V_x - U$, $c_y = V_y - V$ and $c_z = V_z - W$ along the x-, y-, and z-directions, where (U, V, W) corresponds to three components of the mean flow velocity $\vec{U}$.

The BGK equation is an ideal simplified form of the full Boltzmann equation. According to the BGK approximation, the velocity distribution function relaxes towards the Maxwellian distribution with a time constant of $\tau = 1/v_m$. The BGK equation can provide the correct collisionless or free-molecule solution, in which the form of the collision term is immaterial, however, the approximate collision term would lead to an indeterminate error in the transition regime. In the Chapman–Enskog expansion, the BGK model corresponds to the Prandtl number, as the ratio of the coefficient of viscosity μ and heat conduction K

obtained at the Navier–Stokes level, is equal to unity [18], unlike the Boltzmann equation which agrees with experimental data in making it approximately 2/3. Nevertheless, the BGK model has the same basic properties as the Boltzmann collision integral. It is considered [1,7,20,21] that the BGK equation can describe the gas flows in equilibrium or near-equilibrium state.

The BGK model is the simplest model based on relaxation towards Maxwellian. It has been shown from [20,21] that the BGK equation can be improved to better model the flow states far from equilibrium. In order to have a correct value for the Prandtl number, the local Maxwellian f_M in the BGK equation can be replaced by Eq. (1.9.7) from [21], as it leads to the ellipsoidal statistical (ES) model equation [12,37,38]. In this study, the f_M in Eq. (1) is replaced by the local equilibrium distribution function f^N from the Shakov model [13,27,30,39]. The function f^N is taken as the asymptotic expansion in Hermite polynomials with local Maxwellian f_M as the weighting function,

$$f^N = f_M \cdot \left[1 + (1 - Pr)\vec{c} \cdot \vec{q}\left(c^2/(RT) - 5\right)/(5PRT)\right]. \tag{3}$$

Here, Pr is the Prandtl number with $Pr = \mu C_p/K$ and is equal to $2/3$ for a monatomic gas, C_p is the specific heat at constant pressure, and $\vec{q}$ and P, respectively, denote the heat flux vector and gas pressure. It can be shown that if $Pr = 1$ is set in Eq. (3), the BGK model is just recovered with $f^N = f_M$.

According to the relaxation time approximation [1,18,19], the collision frequency v_m in Eq. (1) can be extended and related to the kinetic temperature as a measure of the variance of all thermal velocities in conditions far from equilibrium by using the temperature dependence of the coefficient of viscosity. The nominal collision frequency (inverse relaxation time) can be taken in the form [27,30]

$$v = nkT/\mu, \tag{4}$$

where n is the number density, k is Boltzmann's constant, and $\mu = \mu(T)$ is the coefficient of the viscosity. Since the macroscopic flow parameters at any time at each point of the physical space are derived from moments of f over the velocity space in the kinetic theory of gases, the collision frequency v is variable along with the space $\vec{r}$, time t, and thermal velocity $\vec{c} = \vec{V} - \vec{U}$. Consequently, this collision frequency relationship can be extended and applied to regions of extreme non-equilibrium [7,20,21].

The power law temperature dependence of the coefficient of viscosity can be obtained [7,18] from the Chapman–Enskog theory, which is appropriate for the inverse power law intermolecular force model and the VHS (Variable Hard Sphere) molecular model,

$$\mu/\mu_\infty = (T/T_\infty)^\chi, \tag{5}$$

where χ is the temperature exponent of the coefficient of viscosity that can also be denoted as $\chi = (\zeta + 3/(2(\zeta - 1))$ for the Chapman–Enskog gas of inverse power law, ζ is the inverse power coefficient related to the power force F and the distance r between centers of molecules, that is $F = \kappa/r^\zeta$ with a constant κ.

The viscosity coefficient μ_∞ in the free stream equilibrium can be expressed [7] in terms of the nominal freestream mean free path λ_∞ for a simple hard sphere gas,

$$\mu_\infty = \frac{5}{16} m n_\infty (2\pi R T_\infty)^{1/2} \lambda_\infty. \tag{6}$$

Here, the subscripts ∞ represent the freestream value.

The collision frequency v of the gas molecules can be expressed as the function of density, temperature, the freestream mean free path and the exponent of molecular power law by the combination of Eqs. (4)–(6),

$$v = \frac{16}{5}\sqrt{\frac{R}{2\pi}}\frac{T_\infty^{\chi-1/2}}{n_\infty}\frac{n}{T^{\chi-1}}\frac{1}{\lambda_\infty}. \tag{7}$$

Based on the feature of molecular movement and collision approaching to equilibrium, the BGK equation can be revised by using f^N and v from Eqs. (3) and (7), respectively, to replace f_M and v_m in Eq. (1). The v and the appropriate f^N can be integrated with the flow states, the macroscopic flow parameters, the molecular transport coefficients, the thermodynamic effect and the molecular power law from various flow regimes. Consequently, the non-dimensional form of the unified simplified velocity distribution function equation which qualitatively describes gas flow characteristics from various flow regimes [27,30] can be presented in the Cartesian coordinates:

$$\frac{\partial f}{\partial t} + \vec{V} \cdot \frac{\partial f}{\partial \vec{r}} = v(f^N - f), \tag{8}$$

$$f^N = f_M \cdot \left[1 + (1 - Pr)\vec{c} \cdot \vec{q}\left(2c^2/T - 5\right)/(5PT/2)\right], \tag{9}$$

$$f_M = n/(\pi T)^{3/2} \exp\left[-c^2/T\right], \tag{10}$$

$$v = 8nT^{1-\chi}/\left(5\sqrt{\pi}Kn\right), \tag{11}$$

where Kn is the Knudsen number with $Kn = \lambda_\infty/L$ which is the ratio of the freestream mean free path λ_∞ to the characteristic length L of the problem, all of the variables in Eqs. (8)–(11) or in the following have been non-dimensionalized. Each dimensionless quantity is referred to its freestream equilibrium values at infinity (n_∞, T_∞). The reference speed c_∞ is $\sqrt{2RT_\infty}$, the reference force is $mn_\infty c_\infty^2/2$, the reference heat flux is $mn_\infty c_\infty^3/2$ and the reference time t_∞ is L/c_∞, the reference distribution function is n_∞/c_∞^3.

The macroscopic flow parameters, such as the number density, mean flow velocity, temperature, pressure, viscous stress tensor and heat flux vector, can be determined [1,7,20] from the moments of the velocity distribution function over the molecular velocity space.

$$n(\vec{r}, t) = \int f \, \mathrm{d}\vec{V}, \tag{12}$$

$$nU_i(\vec{r}, t) = \int V_i f \, \mathrm{d}\vec{V}, \tag{13}$$

$$\frac{3}{2} nT(\vec{r}, t) = \int c^2 f \, \mathrm{d}\vec{V}, \tag{14}$$

$$P = nT, \tag{15}$$

$$\tau_{ij}(\vec{r}, t) = 2 \int c_i c_j f \, \mathrm{d}\vec{V} - P\delta_{ij}, \tag{16}$$

$$q_i(\vec{r}, t) = \int c^2 c_i f \, \mathrm{d}\vec{V}, \tag{17}$$

where δ_{ij} is the Kronecker delta, the subscripts i and j each range from 1 to 3. The values 1, 2 and 3 may be identified with components along the x-, y- and z-axes, respectively.

3. Application of the discrete velocity ordinate method in gas kinetic theory

3.1. Development of discrete velocity ordinate method

The discrete ordinate method [40] is based on the representation of functions by a set of discrete points that coincide with the evaluation points in a quadrature rule, which consists of replacing the original functional dependency on the integral variable by a set of functions with N elements $W_i p(x_i)$ $(i = 1, \ldots, N)$, where the points x_i are quadrature points and W_i are the corresponding weights of the integration rule

$$\int_a^b W(x)p(x)\,\mathrm{d}x = \sum_{i=1}^{N} W_i p(x_i). \tag{18}$$

The interval $[a, b]$ will be either $[0, \infty]$ or $[-\infty, \infty]$ for the application considered and a different weight function $W(x)$ is chosen for each problem considered. The x_i are the roots of the Nth-order polynomial $R_n(x)$ of the set that satisfy,

$$\int_a^b W(x)R_n(x)R_i(x)\,\mathrm{d}x = \delta_{in}, \tag{19}$$

where the set of polynomials $R_n(x)$, orthonormal with respect to the weight function $W(x)$ on the interval $[a, b]$, form a complete basis of the $L^2[a, b]$ Hilbert space. The first N of these polynomials form a subspace of this Hilbert space which is isomorphic with the $\Re^N$ Euclidean space. It may be shown from the treatment of the integral over the interval $[a, b]$ with the quadrature rule equation (18) that the discrete ordinate representation is equivalent to the truncated polynomial representation of the Nth-order.

It is shown from [41,42] that, in general, the velocity distribution function f for states removed from equilibrium is proportional to $\exp(-c^2)$ just as it is for equilibrium, that f has finite bounds under the specific precision in the velocity space and tends to zero as c tends to infinity. That is, the integration of the normalized distribution function over all velocity space should yield unity, and the probability of the molecular velocities far removed from the mean velocity $\vec{U}$ of the flow is always negligible. Thus, in order to replace the continuous dependency of the molecular velocity distribution function on the velocity space, the discrete ordinate technique can be introduced to discretize the finite velocity region removed from $\vec{U}$. The choice of the discrete velocity ordinate points in the vicinity of $\vec{U}$ is based only on the moments of the distribution function over the velocity space. Consequently, the numerical integration of the macroscopic flow moments in Eqs. (12)–(17) of the distribution function f over the velocity space can be adequately performed by the same quadrature rule, with f evaluated at only a few discrete velocity points in the vicinity of $\vec{U}$. The selections of the discrete velocity points and the range of the velocity space in the discrete velocity ordinate method are somewhat dependent on the related problems.

Applying the discrete velocity ordinate method to Eq. (8) for the (V_x, V_y, V_z) velocity space, the single velocity distribution function equation can be transformed into hyperbolic conservation equations with nonlinear source terms at each of discrete velocity grid points,

$$\frac{\partial Q}{\partial t} + \frac{\partial F^x}{\partial x} + \frac{\partial F^y}{\partial y} + \frac{\partial F^z}{\partial z} = \bar{S}, \tag{20}$$

with

$$Q = f_{\sigma,\delta,\theta}, \quad F^x = V_{x\sigma}Q, \quad F^y = V_{y\delta}Q, \quad F^z = V_{z\theta}Q, \quad \bar{S} = \nu\left(f^N_{\sigma,\delta,\theta} - f_{\sigma,\delta,\theta}\right),$$

where $f_{\sigma,\delta,\theta}$ and $f^N_{\sigma,\delta,\theta}$, respectively, denote values of f and f^N at the discrete velocity ordinate points $(V_{x\sigma}, V_{y\delta}, V_{z\theta})$, the subscripts σ, δ and θ represent the discrete velocity grid indexes in the V_x-, V_y- and V_z-directions, respectively.

3.2. Study of discrete velocity quadrature methods

Once the discrete velocity distribution functions $f_{\sigma,\delta,\theta}$ are solved, the macroscopic flow moments at any time in each point of the physical space can be obtained and updated by the appropriate discrete velocity quadrature method. In terms of the symmetric quality of the exponential function $\exp(-V^2)$ over the interval $[-\infty,\infty]$, the Gauss–Hermite half-range quadrature [35,43] can be extended to evaluate the infinite integral of the velocity distribution function over all the velocity space. The discrete velocity ordinate points and the weights corresponding to the Gauss–Hermite quadrature can be obtained using the algorithms described by Huang and Giddens [43] and by Shizgal [35], which can be used to approximate the integrals with the exponential type as follows:

$$\int_0^\infty \mathrm{e}^{-V^2} p(V)\,\mathrm{d}V \approx \sum_{\sigma=1}^{N} W_\sigma p(V_\sigma), \tag{21}$$

where V_σ $(\sigma = 1,\ldots,N)$ are the positive roots of the Hermite polynomial of degree N, W_σ are the corresponding weights, the subscript σ is the discrete velocity index and $p(V)$ denote the functions which can be derived from the integrands in Eqs. (12)–(17). According to Kopal's discussion [44], it is known that for a given number of discrete subdivisions of the interval $(0,+\infty)$, the Gauss–Hermite's choice of the discrete velocity points V_σ and the corresponding weights W_σ yields the optimal discrete approximation to the considered integration in the sense. The Gauss–Hermite's V_σ and W_σ can be tabulated in the table of the Gauss–Hermite quadrature. However, the number of the discrete velocity points is limited in this way, as it is very difficult exactly to solve high-order Hermite polynomial. The V_σ and W_σ can also be obtained by directly solving the nonlinear Eqs. (21) and (22) in terms of the decomposing principle,

$$\int_0^\infty \mathrm{e}^{-u^2} u^k\,\mathrm{d}u = \frac{1}{2}\Gamma\left(\frac{k+1}{2}\right). \tag{22}$$

It is shown from the computing practice [45] that it is difficult to ensure the numerical stability with the computation of Eqs. (21) and (22) when the number of discrete velocity points is greatly increased, as indicates that farther application of the Gauss–Hermite quadrature method to high speed gas flows may be restricted.

The advantage of using the modified Gauss–Hermite quadrature formula is its high accuracy, but for high freestream Mach number flows, the number of discrete velocity grid points needed to cover the appropriate velocity range could become quite large. To simulate hypersonic flows, the composite integration method based on equally spaced three-point Newton–Cotes formulas which can be developed by setting the polynomial in the discrete ordinate method as a quadratic interpolating polynomial and the Gauss–Legendre numerical quadrature rule whose integral nodes are determined by using the roots of the kth Legendre polynomials have been applied to this study [45].

When the above-mentioned conventional quadrature methods are used to attack the approximate calculation of multiple integrals, the computational effort and the numerical error will rapidly grow along with the increase of integral overlap number. To raise the precision of solving multiple integrals in multi-dimensional flows and simplify the numerical integration over the discrete velocity space, in particular optimize the distribution of the discrete velocity ordinate points, the algebraic number-theoretic method [46] and the optimum principle [47] of the Golden Section have been extended and applied to the discrete

velocity ordinate method in this study [45]. The discrete velocity points in a direction are determined by the increasing principle with fraction from the number theory and those in other directions are accordingly controlled by the Golden Section method. The rational approximation from Fibonacci number to the golden number ($\omega = (\sqrt{5}-1)/2$) is used

$$\left|\frac{F_{n-1}}{F_n} - \omega\right| < \frac{1}{\sqrt{5}F_n^2}. \tag{23}$$

Here, F_n is the Fibonacci number, which is defined by $F_0 = 0$, $F_1 = 1$ and $F_{n+2} = F_{n+1} + F_n$ ($n \geqslant 0$).

The algebraic number theory of uniform distribution [36] is introduced into the computation of multi-dimensional integrals. The Hua-Wang's method [48] in which the multi-integral is approximated by single summation is employed. As a result, the Golden Section number-theoretic integral formula can be developed to evaluate the macroscopic flow moments over the velocity space in terms of the intrinsic relation between the asymptotic fraction (that is $0/1, 1/1, 1/2, 2/3, 3/5, 5/8, 8/13, \ldots, F_n/F_{n+1}, \ldots$) of the golden number and the numerical integral. In particular, the double-integral with the integrand $Q(x, y)$ can be evaluated by

$$\int_0^1 \int_0^1 Q(x,y)\,\mathrm{d}x\,\mathrm{d}y \approx \frac{1}{F_m}\sum_{k=1}^{F_m} Q\left(\frac{k}{F_m}, \left\{\frac{F_{m-1}k}{F_m}\right\}\right), \tag{24}$$

where $\{\xi\}$ denotes the fractional portion of the rational number ξ.

The ternary-integral with the integrand $Q(x, y, z)$ can be evaluated by single summation,

$$\int_0^1 \int_0^1 \int_0^1 Q(x,y,z)\,\mathrm{d}x\,\mathrm{d}y\,\mathrm{d}z \approx \frac{1}{n}\sum_{k=1}^{n} Q\left(\frac{k}{n}, \left\{\frac{h_1 k}{n}\right\}, \left\{\frac{h_2 k}{n}\right\}\right), \tag{25}$$

where (h_1, h_2, n) can be taken as the extension on the collection of Fibonacci integer number sequence, which can be referred by the table of the lattice point collection from [36]. It can be shown that the number n of discrete ordinate points need to be greatly increased to diminish the error between the numerical quadrature and the original integral and simulate high-speed gas flows, however, a great deal of computer storage will be expected to store the discrete velocity distribution functions at those points.

4. Numerical algorithm for the velocity distribution function equations

4.1. Numerical method for one-dimensional gas flows

In order to reduce the computer storage requirement, the velocity distribution function equation can be accurately integrated on the velocity components in some directions with appropriate weighting factors, where the components of macroscopic flow velocity are zero. Consequently, the reduced distribution functions can be introduced to cut back the number of independent variables in the distribution function f in Eq. (8). For problems in one space dimension, say x, a great simplification is possible through the following reduction procedure. Two reduced distribution functions of the x, velocity component V_x and time t are defined [49]:

$$g(x, V_x, t) = \int_{-\infty}^{\infty}\int_{-\infty}^{\infty} f(x, V_x, V_y, V_z, t)\,\mathrm{d}V_y\,\mathrm{d}V_z, \tag{26}$$

$$h(x, V_x, t) = \int_{-\infty}^{\infty}\int_{-\infty}^{\infty}\left(V_y^2 + V_z^2\right) f(x, V_x, V_y, V_z, t)\,\mathrm{d}V_y\,\mathrm{d}V_z. \tag{27}$$

Now integrating out the V_y and V_z dependence on Eq. (8) in describing one-dimensional gas flows, the following equivalent system to Eq. (8) is got:

$$\frac{\partial g}{\partial t} + V_x\frac{\partial g}{\partial x} = v\left(G^N - g\right), \tag{28}$$

$$\frac{\partial h}{\partial t} + V_x\frac{\partial h}{\partial x} = v\left(H^N - h\right), \tag{29}$$

where

$$\begin{aligned} G^N &= G_{\mathrm{M}}\left\{1 + (1-Pr)(V_x - U)q_x\left[2(V_x-U)^2/T - 3\right]\Big/(5PT/2)\right\},\\ G_{\mathrm{M}} &= n/(\pi T)^{1/2}\exp\left[-(V_x-U)^2/T\right], \end{aligned} \tag{30}$$

$$\begin{aligned} H^N &= H_{\mathrm{M}}\left\{1 + (1-Pr)(V_x - U)q_x\left[2(V_x-U)^2/T - 1\right]\Big/(5PT/2)\right\},\\ H_{\mathrm{M}} &= T\cdot G_{\mathrm{M}}. \end{aligned} \tag{31}$$

The macroscopic flow parameters denoted by the reduced distribution functions can be similarly obtained by substituting Eqs. (26) and (27) into Eqs. (12)–(17).

Thus, the molecular velocity distribution function equation for one-dimensional gas flows can be transformed into two simultaneous equations on the reduced distribution functions instead of one single equation and can be cast into the following conservation law form recurring to the discrete velocity ordinate method described in the Section 3.

$$\frac{\partial \mathbf{U}}{\partial t} + \frac{\partial \mathbf{F}}{\partial x} = \mathbf{S}, \tag{32}$$

with

$$\mathbf{U} = \begin{pmatrix} g_\sigma \\ h_\sigma \end{pmatrix}, \quad \mathbf{F} = V_{x\sigma}\mathbf{U}, \quad \mathbf{S} = \begin{pmatrix} v\left(G_\sigma^N - g_\sigma\right) \\ v\left(H_\sigma^N - h_\sigma\right) \end{pmatrix},$$

where g_σ, h_σ, G_σ^N and H_σ^N correspond to the values of g, h, G^N and H^N at the discrete velocity grid points $V_{x\sigma}$, respectively.

Using the NND scheme [33] with the second-order Runge–Kutta method in temporal integral, the finite difference second-order scheme is constructed:

$$\begin{aligned} &\delta_t\mathbf{U}^* = R(\mathbf{U}^n),\\ &\mathbf{U}^* = \mathbf{U}^n + \Delta t\cdot\delta_t\mathbf{U}^*,\\ &\delta_t\mathbf{U}^{**} = R(\mathbf{U}^*),\\ &\mathbf{U}^{n+1} = \mathbf{U}^n + \frac{\Delta t}{2}\cdot\left(\delta_t\mathbf{U}^* + \delta_t\mathbf{U}^{**}\right). \end{aligned} \tag{33}$$

The operator $R(\mathbf{U}^n)$ is defined by

$$R(\mathbf{U}^n) = -\tfrac{1}{\Delta x}\left(\mathbf{H}^n_{i+1/2} - \mathbf{H}^n_{i-1/2}\right) + \mathbf{S}^n_i,$$

with the numerical flux defined by

$$\mathbf{H}_{i+1/2} = \mathbf{F}^+_i + \tfrac{1}{2}\mathrm{minmod}\left(\Delta\mathbf{F}^+_{i-1/2}, \Delta\mathbf{F}^+_{i+1/2}\right) + \mathbf{F}^-_{i+1} - \tfrac{1}{2}\mathrm{minmod}\left(\Delta\mathbf{F}^-_{i+1/2}, \Delta\mathbf{F}^-_{i+3/2}\right),$$

and the minmod operator is defined by

$$\mathrm{minmod}(x, y) = \tfrac{1}{2}[\mathrm{sgn}(x) + \mathrm{sgn}(y)] \cdot \min(|x|, |y|).$$

The stable condition of the scheme can be written as

$$\Delta t_{\mathrm{S}} = \mathrm{CFL} \Big/ \left(\frac{v}{2} + \frac{3}{2}\frac{|V_{x\sigma}|}{\Delta x}\right)_{\max},$$

where the CFL number is set equal to 0.95. For accuracy, the time step should be less than the local characteristic collision time $\Delta t_{\mathrm{C}} = 1/v_{\max}$ [7,50]. Thus,

$$\Delta t = \min\left(\Delta t_{\mathrm{C}}, \Delta t_{\mathrm{S}}\right). \tag{34}$$

4.2. Numerical algorithm for two-dimensional gas flows

For analyses of gas flows in x and y directions around two-dimensional bodies, the molecular velocity distribution function equation in Eq. (8) can be integrated with respect to V_z with weighting factors 1 and V_z^2 so that the number of independent variables is reduced by integrating out the dependence of f on V_z. The following reduced distribution functions are introduced [27,30,32]:

$$g(x, y, t, V_x, V_y) = \int_{-\infty}^{\infty} f(x, y, t, V_x, V_y, V_z)\,\mathrm{d}V_z, \tag{35}$$

$$h(x, y, t, V_x, V_y) = \int_{-\infty}^{\infty} V_z^2 f(x, y, t, V_x, V_y, V_z)\,\mathrm{d}V_z. \tag{36}$$

After substituting Eqs. (35) and (36) into Eq. (8) describing two-dimensional gas flows, and applying the discrete velocity ordinate method to velocity components V_x and V_y, the single velocity distribution function equation can become into two simultaneous equations with the hyperbolic conservation law form in the transformed coordinates (ξ, η) as follows:

$$\frac{\partial \mathbf{U}}{\partial t} + \frac{\partial \mathbf{F}}{\partial \xi} + \frac{\partial \mathbf{G}}{\partial \eta} = \mathbf{S}, \tag{37}$$

with

$$\mathbf{U} = J\begin{pmatrix} g_{\sigma,\delta} \\ h_{\sigma,\delta} \end{pmatrix}, \quad \mathbf{F} = \bar{U}\mathbf{U}, \quad \mathbf{G} = \bar{V}\mathbf{U}, \quad \mathbf{S} = J\begin{pmatrix} v(G^N_{\sigma,\delta} - g_{\sigma,\delta}) \\ v(H^N_{\sigma,\delta} - h_{\sigma,\delta}) \end{pmatrix},$$

where $g_{\sigma,\delta}$, $h_{\sigma,\delta}$, $G^N_{\sigma,\delta}$ and $H^N_{\sigma,\delta}$ denote values of g, h, G^N and H^N at the discrete velocity points $(V_{x\sigma}, V_{y\sigma})$, respectively,

$$\begin{aligned} G^N &= G_{\mathrm{M}}\left[1 + (1 - Pr)(c_i q_i)\left(2c^2/T - 4\right)/(5PT/2)\right], \\ G_{\mathrm{M}} &= \frac{n}{\pi T}\exp\left(-c^2/T\right), \end{aligned} \tag{38}$$

$$\begin{aligned} H^N &= H_{\mathrm{M}}\left[1+(1-Pr)(c_i q_i)\left(2c^2/T-2\right)/(5PT/2)\right],\\ H_{\mathrm{M}} &= TG_{\mathrm{M}}/2,\\ c^2 &= (V_x-U)^2+\left(V_y-V\right)^2,\\ c_i q_i &= (V_x-U)q_x+\left(V_y-V\right)q_y. \end{aligned} \tag{39}$$

Note that $\bar{U}$, $\bar{V}$ are the so-called "contravariant molecular velocity" defined as $\bar{U}=V_{x\sigma}\xi_x+V_{y\delta}\xi_y$, $\bar{V}=V_{x\sigma}\eta_x+V_{y\delta}\eta_y$, J is the Jacobian of the general transformation, that is $J=\partial(x,y)/\partial(\xi,\eta)$. The Jacobian coefficient matrices $A=\partial F/\partial U$ and $B=\partial G/\partial U$ of the transformed equation (37) are diagonal and have real eigenvalues $a=\bar{U}$ and $b=\bar{V}$.

In view of the unsteady characteristic of molecular convective movement and colliding relaxation, the time-splitting method [45,51] is used to divide Eq. (37) into the colliding relaxation equations with the nonlinear source terms and the convective movement equations. Considering simultaneously proceeding on the molecular movement and colliding relaxation in real gas, the computing order of the previous and hind time steps is interchanged to couple to solve them in the computation. The finite difference second-order scheme is developed by using the improved Euler method and the NND-4(a) scheme [34] which is a two-stage scheme with second-order accuracy in time and space,

$$\mathbf{U}^{n+1}=L_{\mathrm{S}}(\Delta t/2)L_\eta(\Delta t/2)L_\xi(\Delta t)L_\eta(\Delta t/2)L_{\mathrm{S}}(\Delta t/2)\mathbf{U}^n, \tag{40}$$

where

$$\mathbf{U}^*=L_{\mathrm{S}}(\Delta t)\mathbf{U}^n=\mathbf{U}^n+\left(1-\frac{v}{2}\Delta t\right)\Delta t\cdot\mathbf{S}^n, \tag{41}$$

$$\mathbf{U}^{**}=L_\eta(\Delta t)\mathbf{U}^*=\left[1-b\Delta t\delta_\eta+\frac{b^2\Delta t^2}{2}\delta_{\eta^2}\right]\mathbf{U}^*, \tag{42}$$

$$\mathbf{U}^{n+1}=L_\xi(\Delta t)\mathbf{U}^{**}=\left[1-a\Delta t\delta_\xi+\frac{a^2\Delta t^2}{2}\delta_{\xi^2}\right]\mathbf{U}^{**}. \tag{43}$$

The integration operator $L_{\mathrm{S}}(\Delta t)$ for the colliding relaxation source terms is done using the improved Euler method. The one-dimensional space operators $L_\eta(\Delta t)$ and $L_\xi(\Delta t)$, respectively, corresponding to the convective movement terms $\partial G/\partial\eta$ and $\partial F/\partial\xi$ are approximated by the NND-4(a) scheme. The Δt in the computation can be chosen [45] as

$$\Delta t=\min(\Delta t_{\mathrm{C}},\Delta t_{\mathrm{S}}).$$

Here, $\Delta t_{\mathrm{S}}=\mathrm{CFL}/\max(v/2,|\bar{U}|/\Delta\xi,|\bar{V}|/\Delta\eta)$.

4.3. Numerical algorithm for three-dimensional gas flows

For the three-dimensional gas flows, the molecular velocity distribution function remains to be a function of seven independent variables in the phase space. The discrete velocity ordinate method can be applied to the velocity distribution function in Eq. (8) to remove its continuous dependency on velocity components (V_x,V_y,V_z), as described in Section 3.1. Moreover, to treat arbitrary geometry configuration, the body fitted coordinate is introduced. By applying the general transformation technique, Eq. (20) on the discrete velocity distribution functions can be written in the transformed coordinates (ξ,η,ζ) [45] as:

$$\frac{\partial U}{\partial t}+\frac{\partial F}{\partial \xi}+\frac{\partial G}{\partial \eta}+\frac{\partial H}{\partial \zeta}=S, \tag{44}$$

with

$$U=JQ,\quad F=\bar{U}U,\quad G=\bar{V}U,\quad H=\bar{W}U,\quad S=J\bar{S},$$

where $\bar{U}=V_{x\sigma}\xi_x+V_{y\delta}\xi_y+V_{z\theta}\xi_z$, $\bar{V}=V_{x\sigma}\eta_x+V_{y\delta}\eta_y+V_{z\theta}\eta_z$, $\bar{W}=V_{x\sigma}\zeta_x+V_{y\delta}\zeta_y+V_{z\theta}\zeta_z$ and $J=\partial(x,y,z)/\partial(\xi,\eta,\zeta)$.

Drawing on the decoupling technique [7,52] on molecular movement and colliding in the DSMC method, the time-splitting method for the unsteady equation has been developed to split up Eq. (44) into the colliding relaxation equations with the nonlinear source terms and the convective movement equations in three directions so as to couple to solve them in the computation [45,53]. The colliding relaxation equations with the nonlinear source terms are numerically simulated by the second-order Runge–Kutta method. The NND-4(a) scheme [54] based on primitive variables is used numerically to solve the convective movement equations. Adhering to the gas kinetic theory, the finite difference second-order scheme directly solving the discrete velocity distribution functions is constructed as

$$U^{n+1}=L_{\mathrm{S}}\left(\frac{\Delta t}{2}\right)L_{\zeta}\left(\frac{\Delta t}{2}\right)L_{\eta}\left(\frac{\Delta t}{2}\right)L_{\xi}(\Delta t)L_{\eta}\left(\frac{\Delta t}{2}\right)L_{\zeta}\left(\frac{\Delta t}{2}\right)L_{\mathrm{S}}\left(\frac{\Delta t}{2}\right)U^{n}, \tag{45}$$

where

$$U^{*}=L_{\mathrm{S}}(\Delta t)U^{n}=U^{n}+\Delta t(1-v\Delta t/2)S^{n}, \tag{46}$$

$$U^{**}=L_{\zeta}(\Delta t)U^{*}=\left[1-c\Delta t\delta_{\zeta}+\frac{c^2\Delta t^2}{2}\delta_{\zeta^2}\right]U^{*}, \tag{47}$$

$$U^{***}=L_{\eta}(\Delta t)U^{**}=\left[1-b\Delta t\delta_{\eta}+\frac{b^2\Delta t^2}{2}\delta_{\eta^2}\right]U^{**}, \tag{48}$$

$$U^{n+1}=L_{\xi}(\Delta t)U^{***}=\left[1-a\Delta t\delta_{\xi}+\frac{a^2\Delta t^2}{2}\delta_{\xi^2}\right]U^{***}. \tag{49}$$

Here, $a=\bar{U}$, $b=\overline{V}$ and $c=\bar{W}$.

Based on the molecular collision spacing theory, the time step size (Δt) in the computation should be less than the local mean collision time space (Δt_{C}) [7,50], thus

$$\Delta t=\min(\Delta t_{\mathrm{C}},\Delta t_{\mathrm{S}}),$$

where the stable condition [45] of the scheme can be written as

$$\Delta t_{\mathrm{S}}=\mathrm{CFL}/\max\left(v/2,|\bar{U}|/\Delta\xi,|\bar{V}|/\Delta\eta,|\bar{W}|/\Delta\zeta\right). \tag{50}$$

4.4. Boundary conditions and its numerical procedure

For the interaction of molecules with the body surface, perfect diffuse reflection is assumed [20,27,30,45]. That is, molecules which strike the wall surface are subsequently emitted with the Maxwellian velocity distribution fully accommodating to the wall temperature T_{w} and velocity $(U_{\mathrm{w}},V_{\mathrm{w}},W_{\mathrm{w}})$. The velocity distribution function reflected from the wall surface in the discrete form is set as [45]

$$f^{w}_{\sigma,\delta,\theta} = \frac{n_{\mathrm{w}}}{(\pi T_{\mathrm{w}})^{3/2}} \exp\left[- \frac{(V_{x\sigma} - U_{\mathrm{w}})^2 + (V_{y\delta} - V_{\mathrm{w}})^2 + (V_{z\theta} - W_{\mathrm{w}})^2}{T_{\mathrm{w}}} \right]. \tag{51}$$

The number density of molecules diffusing from the surface, n_{w}, which is not known previously, is determined from the mass balance condition on the surface. One has

$$n_{\mathrm{w}} = -2\left(\frac{\pi}{T_{\mathrm{w}}}\right)^{1/2} \int_{c_n<0} c_n^{-} \cdot f \, \mathrm{d}\vec{V}, \tag{52}$$

where $c_n^{-} = (c_n - |c_n|)/2$, $c_n = \vec{c} \cdot \vec{n}$, and $\vec{n}$ is the outward unit vector normal to the solid surface.

The distribution function is assumed to be in equilibrium at infinity. However, the outer boundary must be in some finite distance from the body, so the outer boundary conditions are treated using characteristics-based boundary conditions. The distribution function for outgoing molecules through boundaries is determined in terms of the condition which is in accord with the upwind nature of the interior point scheme [45]. For molecules incoming from outside, along with the inlet boundary ahead of the shock wave, the distribution function is given by the equilibrium distribution with prescribed free stream properties from upstream [51], however, on the outlet boundary, it is assumed that there is no gradient along the outward direction for the distribution function [45].

For problems with symmetry, the half flow field is only computed to save the computer memory by the way where the cells on the symmetrical line (plane) of the flow field are processed as interior points and the symmetry conditions are enforced and assigned to the distributions function along the symmetrical line (plane) of the flow field [45].

5. Numerical examples of gas flows from various flow regimes

To test the accuracy and efficiency of the present numerical method in solving the gas dynamical problems from rarefied flow to continuum, the one-dimensional shock-tube problems, the flows past two-dimensional circular cylinder and the flows past three-dimensional sphere with various Knudsen numbers are simulated in the serial computer. In the computation, the convergence of a steady-state solution is assumed to have occurred when the quadratic global relative error of the flow quantities (e.g., density, flow velocity and temperature), which are evaluated by the discrete velocity numerical integration methods described in Section 3, between successive iteration steps is less than 10^{-4}.

5.1. One-dimensional shock-tube problems with various Knudsen numbers

5.1.1. Unsteady Riemann shock-tube problem

The Riemann shock-tube problem, which has been numerically studied by Chu [49], Reitz [23], Prendergast and Xu [24,26], etc. can be described by the way where a diaphragm located at $x = 0.5$ divides a one-dimensional flow field into two regions, each in a constant equilibrium state at $t = 0$. Here, to test the present numerical method, a case is considered with initial states: $\rho = 0.445,\ T = 13.21,\ U = 0.698$ for $0.0 \leqslant x \leqslant 0.5$ and $\rho = 0.5,\ T = 1.9,\ U = 0.0$ for $0.5 < x \leqslant 1$. The ratio of specific heats γ is 5/3 for a monatomic Maxwell gas. The cell size $\Delta x = 0.01$ in the physical space was set and the six-points Gauss–Legendre numerical quadrature rule with the discrete velocity sub-spacing $\Delta V = 2.0$ was employed to evaluate the macroscopic flow moments over the velocity space, which has 61 discrete velocity grid points ranging from -10 to 10. To see the effects of various Knudsen numbers on the shock-tube flow, the cases of $Kn = 0.0001,\ 0.001,\ 0.005,\ 0.01,\ 0.1$ have been computed, where the computing time step (Δt) was determined by Eq. (34). Figs. 1 and 2, respectively, show the computational results (denoted as symbols) of

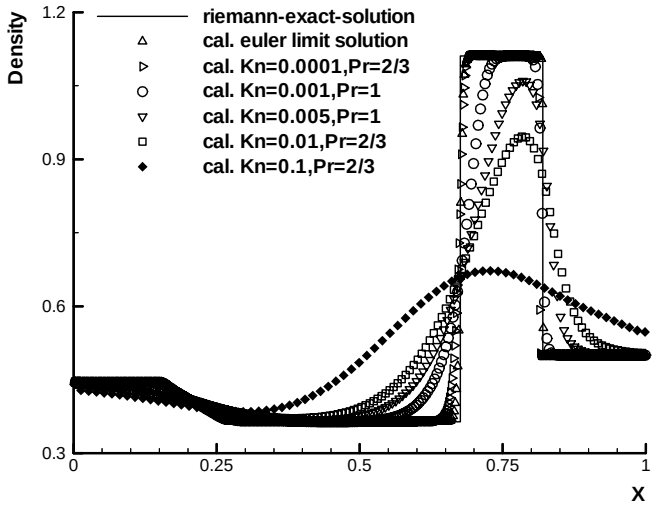

Fig. 1. Density profiles of Riemann shock-tube problem for various *Kn*.

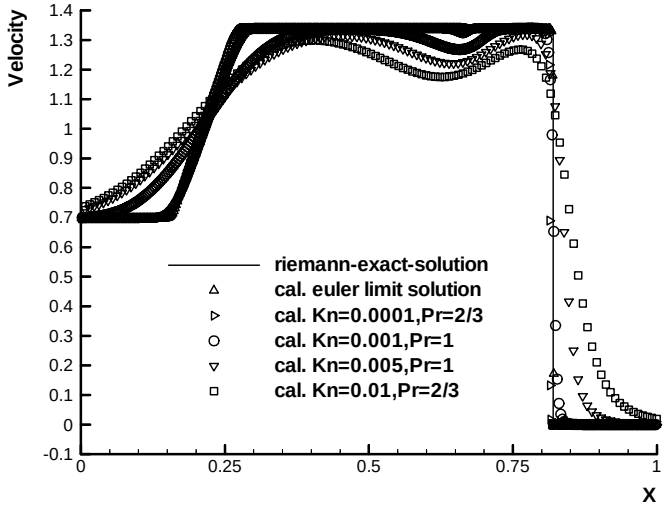

Fig. 2. Velocity profiles of Riemann shock-tube problem for various *Kn*.

density and flow velocity profiles at time $t = 0.1314$. To see the contribution of the collision integral term in the Boltzmann equation to the velocity distribution function, we test a numerical method which is generated from Eq. (8) by neglecting the colliding relaxation source term and setting the distribution function in convective term equal to the equilibrium Maxwellian distribution ($f = f_{\mathrm{M}}$). The solution obtained by such a scheme is named as the Euler limit solution of continuum flow. In Figs. 1 and 2, the solid line denotes the Riemann exact solution of inviscid gas dynamics, the symbols ($\triangle$) denote the computed Euler limit solution, the symbols ($\triangleright$) denote the computed $Kn = 0.0001$, $Pr = 2/3$ results, the symbols ($\bigcirc$) denote the computed $Kn = 0.001$, $Pr = 1$ results, the symbols (∇) denote the computed $Kn = 0.005$, $Pr = 1$ results,

the symbols (□) denote the computed $Kn = 0.01$, $Pr = 2/3$ results and the symbols (◆) denote the computed $Kn = 0.1$, $Pr = 2/3$ results. It is shown that the bigger the Knudsen number becomes from $Kn = 0.0001$ to $Kn = 0.1$, the thicker is the shock and expansion wave, and the rarefied flow corresponding to $Kn = 0.1$ only exists strong disturbance without the shock or expanding wave. The smaller is the Knudsen number, the crisper shock and expanding wave profiles are given. The results appropriate to $Kn = 0.0001$ are in good agreement with the computed Euler limit solution and the exact solution of gas dynamics. The computed velocity profiles also show a particular phenomenon that the computed flow velocity near the contact discontinuity surface deviates from the exact solution of inviscid gas dynamics, the deviation is becoming more prominent with increasing Knudsen number, and the deviation gradually vanishes when the Knudsen number diminishes down to $Kn = 0.0001$. The deviation near the contact surface shows the non-equilibrium effects of the rarefied gas flows with various Knudsen numbers in the shock tube, as may be induced from the conservation of the total momentum in the tube. Figs. 1 and 2 qualitatively reveal the changing process that the gas flow becomes from rarefied flow to continuum along with diminishing the Knudsen number.

5.1.2. SOD shock-tube problem

To test the present numerical method and show the effect of rarefaction in the shock tube flow, the SOD shock-tube problem is set with initial states: $\rho = 10,\ T = 1.667,\ U = 0.0$ for $0.0 \leqslant x \leqslant 0.5$ and $\rho = 1,\ T = 1.333,\ U = 0.0$ for $0.5 < x \leqslant 1$. The computation was gone along the physical spacing $\Delta x = 0.01$ and the composite Newton–Cotes quadrature formula with 101 discrete velocity ordinate points ranging from -6 to 9. The computed results of pressure and temperature for the cases of $Kn = 0.001,\ 0.01,\ 0.1, Pr = 1$ at time $t = 0.1912$ are, respectively, shown in Figs. 3 and 4 accompanying the comparisons with the exact solutions obtained using the Euler equations of gas dynamics of continuum flow. In Figs. 3 and 4, the solid line denotes the Euler exact solution of the SOD shock-tube problem, the symbols (■) denote the computed $Kn = 0.001$ results, the symbols (○) denote the computed $Kn = 0.01$ results and the symbols (▽) denote the computed $Kn = 0.1$ results. It is shown that the distinct shock and rarefaction wave is gradually forming, and the profiles of the computed pressure and temperature approach to the Euler exact solutions of the continuum flow while the Knudsen number decreases from $Kn = 0.1$ to 0.001. There is no shock and expanding wave, but strong disturbance for the fully rarefied flow related to the state $Kn = 0.1$ only exists.

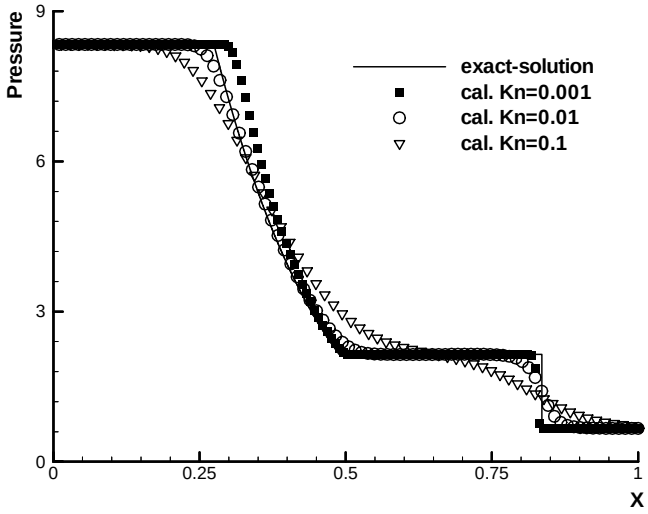

Fig. 3. Pressure profiles of SOD shock-tube problem for various *Kn*.

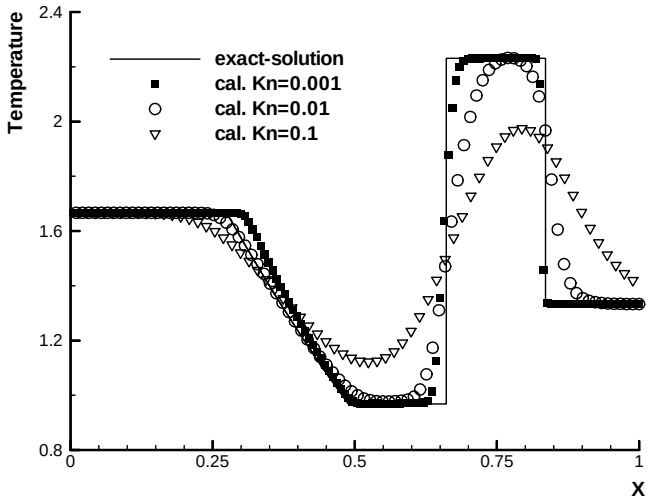

Fig. 4. Temperature profiles of SOD shock-tube problem for various *Kn*.

The above-mentioned phenomena are only the representation of the notable differences between continuum and rarefied flows, which are aroused by the difference of molecular transport capability from various flow regimes.

5.2. The normal shock-structure problems for different Mach numbers

In the case of the normal shock wave, there is no stream speed in the plane of the wave, and the transition is from a supersonic upstream (state1) flow to a subsonic downstream (state2) flow. The shock Mach number M_S is defined as the ratio of the speed of the wave, relative to the upstream gas, to the speed of sound in this gas. The upstream state is chosen as the reference state with $\rho_1 = 1$, $T_1 = 1$ and $P_1 = 1$. The relations of the flow states (upstream $\rho_1,\ T_1,\ U_1$ and downstream $\rho_2,\ T_2,\ U_2$) across the wave are defined in terms of the Rankine–Hugoniot conditions. The flow region is extended over a distance $-x_1 < x < x_2$. A discontinuity between upstream and downstream states was set at $x = 0$ as the initial condition.

To demonstrate the reliability of the present algorithm in solving the shock structure problems for different shock Mach numbers, the cases of $M_S = 1.2,\ 1.55,\ 8,\ 9$ for argon gas have been computed with $Pr = 2/3$, $\gamma = 5/3$. The computed results for the density and temperature profiles are, respectively, compared with the experimental data [55], N–S predictions and DSMC results [7] in Figs. 5–8, where the line denotes the computed results and the symbols denote the aforementioned reference data. The density is normalized in terms of the densities ρ_1 and ρ_2 in front of and behind the shock wave as indicated. The normalized values of the temperature are defined in a similar manner. The length scale is normalized by the mean free path (λ_1) in front of the shock wave. The quoted mean free path is defined in terms of the coefficient of viscosity by Eq. (4.52) in [7]. The molecular model parameters for argon are employed from Appendix A in [7]. The origin has been set at the point in the profile when the density is midway between the upstream and downstream values. Fig. 5 presents the comparison of the computed low Mach number density profiles corresponding to the viscosity-temperature index $\chi = 0.81$ and the shock Mach number $M_S = 1.2$ with the results of the Navier–Stokes theory, as this theory is generally supposed to be accurate for shock Mach numbers less than 2. The space grid points used are 321 with $\Delta x = 0.25\lambda_1$, and the modified Gauss–Hermite quadrature rule with 16 discrete points is employed in the discrete velocity space. It is found

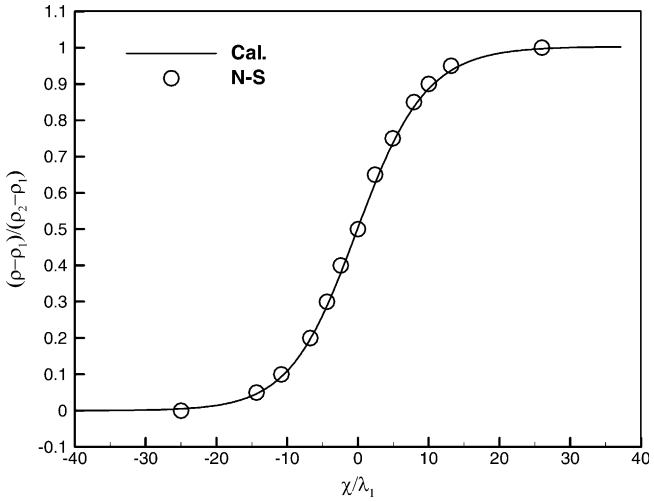

Fig. 5. Comparison of computed density profile with N–S solution for $M_S = 1.2$.

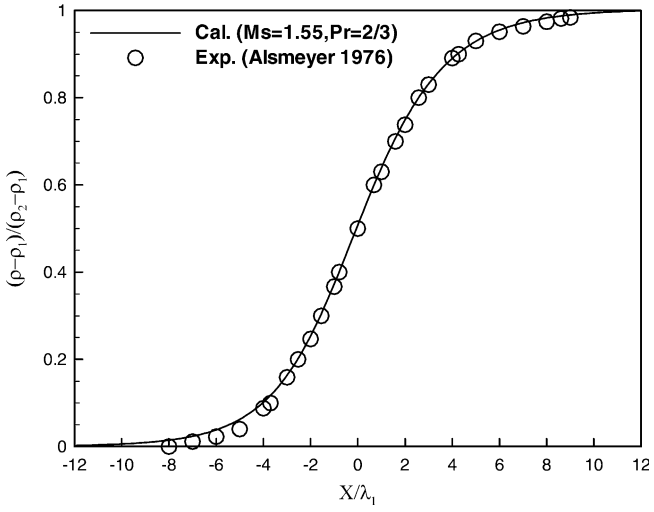

Fig. 6. Comparison of computed density profile with experimental data for $M_S = 1.55$.

that the present kinetic solutions are in fact very close to the N–S solutions for this very weak wave. For the case of $M_S = 1.55$, $\chi = 0.81$, Fig. 6 compares the computed density profiles with Alsmeyer's experimental values from [55]. Overall, the excellent agreement is found.

In the computation of cases of $M_S = 8, 9$, the space grid points used are 121 with $\Delta x = 0.25\lambda_1$, and the Newton–Cotes quadrature formula was employed to evaluate the macroscopic flow moments with 121 discrete velocity ordinate points using the discrete velocity spacing $\Delta V = 0.35$. The coefficient of gas viscosity has been assumed as the power law temperature dependence, that is $\mu \propto T^{\chi}$. The viscosity–temperature index χ should be given variously with the different range of temperature, that is in $[0.72, 0.81]$ for argon gas. The χ value should decrease when the gas temperature increases. The value of $\chi = 0.81$ is appropriate at the temperature near the standard conditions. Here, the viscosity index is set as $\chi = 0.75$ for

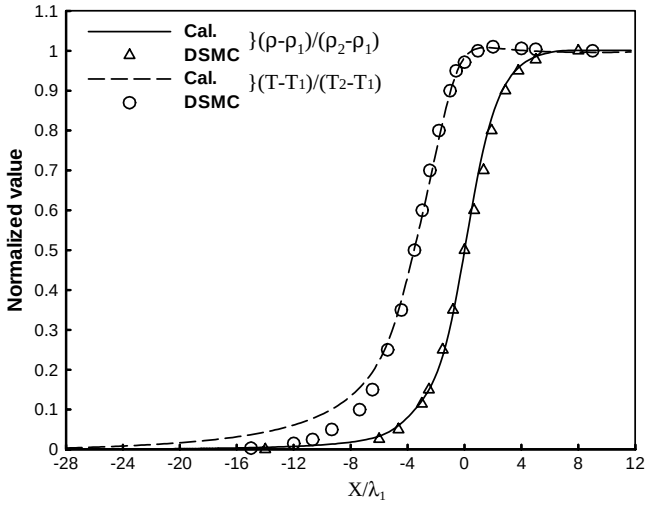

Fig. 7. Comparison of computed temperature and density profiles with DSMC results for $M_S = 8$.

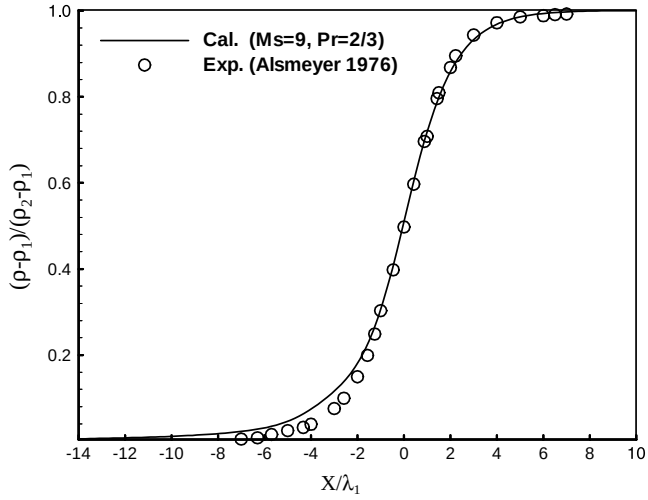

Fig. 8. Comparison of computed density profile with experimental data for $M_S = 9$.

the case of shock Mach number $M_S = 8$, and χ is set as 0.72 for the case of $M_S = 9$. In Fig. 7, the computed results of the normalized density and temperature profiles for the case of $M_S = 8$, $\chi = 0.75$ are, respectively, compared with the Bird's DSMC simulations from [7]. The overall agreement is good and the agreement of density is better than the temperature between the DSMC results and the present calculation. As the shock becomes stronger, some qualitative changes to the shock profiles have been shown in Fig. 7, that is a marked asymmetry in the profiles and an overshoot of about 1% in the temperature at the back of the wave. The asymmetry is also accentuated by a region at the front of the wave where the density is essentially equal to the upstream value, but where there is a significant increase in temperature. Fig. 8 shows the comparison of the present computed density profiles and Alsmeyer's experimental data from [55] for the case of $M_S = 9$,

$\chi = 0.72$. Overall, the two sets of results are in good agreement for this higher Mach number flow. However, on the low-pressure side of the shock wave, the computed results show some deviation from the experimental results and approach the conditions at infinity more slowly.

The viscous shear stress and heat flux vector are sensitive quantities inside the shock, which are defined by Eqs. (16) and (17). To see the variation of the viscous stress and heat flux inside the shock structure with different shock Mach numbers, Figs. 9 and 10, respectively, show the viscous stress and heat flux profiles in the x-direction for the above cases of $M_S = 1.2$ and 9, where the symbols (○) denote the computed viscous stress in the x-direction and the symbols (△) denote the computed heat flux in the negative x-direction. The origin has been set at the point in the profile where the density is midway. It can be shown from Figs. 9 and 10, for the low Mach number ($M_S = 1.2$) shock structure almost in the continuum regime, the profiles of the

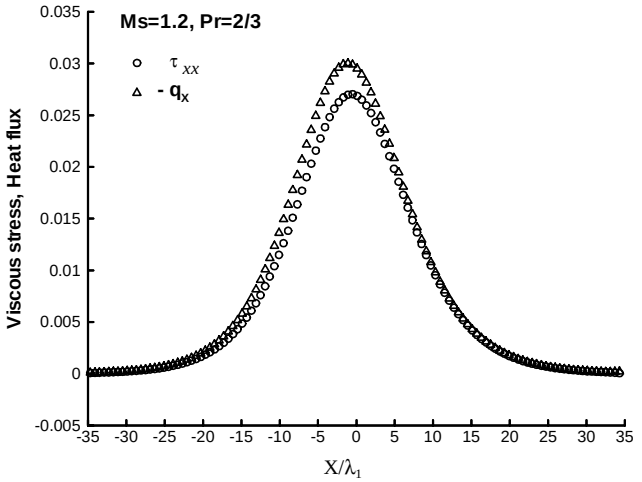

Fig. 9. Viscous stress and heat flux profiles in x-direction for $M_S = 1.2$.

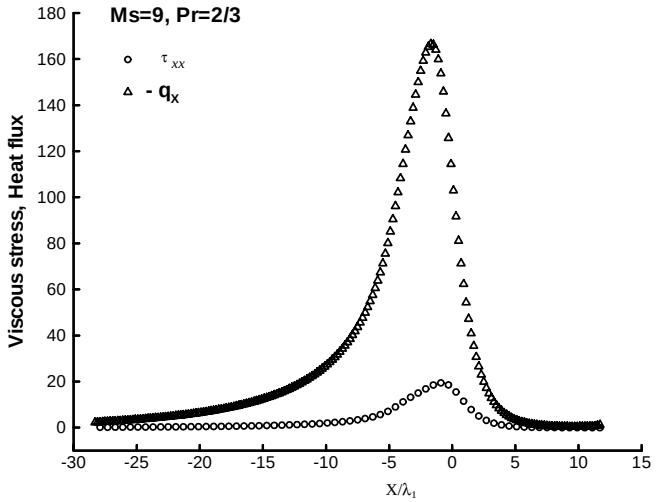

Fig. 10. Viscous stress and heat flux profiles in x-direction for $M_S = 9$.

viscous stress and heat flux only have a little deviation from the symmetric equilibrium distribution based on the center of the wave. However, for the high Mach number ($M_S = 9$) shock flow in the rarefied regime, prominent asymmetric distribution appears in the profiles, the peak of the profiles is far from the center of the wave, the significant increase in the heat flux is accentuated by a region at the front of the wave, as the transport of the kinetic energy represented by the heat flux is late to the transport of the momentum represented by the shear stress in the normal shock wave flow.

5.3. Two-dimensional supersonic flows past cylinder from rarefied regime to continuum

The steady supersonic flows past a circular cylinder under various free-stream Mach (M_∞) and Knudsen numbers are computed. Here, due to symmetry, only half plane on the cylinder is considered and symmetry boundary conditions were employed. The mesh system used is 71×51 (streamwise $\times$ surface normal) in the physical space and the modified Gauss–Hermite quadrature formula with 32×16 discrete velocity ordinate points was employed. The computational results of the pressure and Mach number contours are shown in Figs. 11 and 12, respectively, respected to the states of $M_\infty = 1.8$, $Pr = 2/3$, $\gamma = 5/3$, the ratio $T_w/T_0 = 1$ of the wall temperature to the total temperature, $Kn = 1,\ 0.1,\ 0.03$ and $Kn = 0.001$ ($M_\infty = 4$). It is shown in Figs. 11 and 12 that there is no shock wave disturbing region for the fully rarefied flow related to $Kn = 1$, however, the strong disturbing domain and the dim bow shock appear in the rarefied transition flows related to $Kn = 0.1$ and $Kn = 0.03$, and for the near continuum flow of $Kn = 0.001$, the flow structures including the front bow shock, stagnation region and near wake are well captured. The smaller is the Knudsen number, the thinner and clearer is the bow shock occurring in front of the body. It is qualitatively shown from Figs. 11 and 12 that the gas flow approaches to continuum flow from rarefied transition flow while the Knudsen number is diminishing from $Kn = 1$ to $Kn = 0.001$.

To try out the computation of the present algorithm to the two-dimensional continuum flow, the case of $Kn = 0.0001$, $M_\infty = 1.8$, $Pr = 2/3$, $T_w = T_0$ and $\gamma = 5/3$ in the continuum flow regime was set with the 71×51 space cells and the modified Gauss–Hermite quadrature formula with 32×16 discrete points. The computed results of pressure, density, temperature, Mach number contours and wake flow structures are

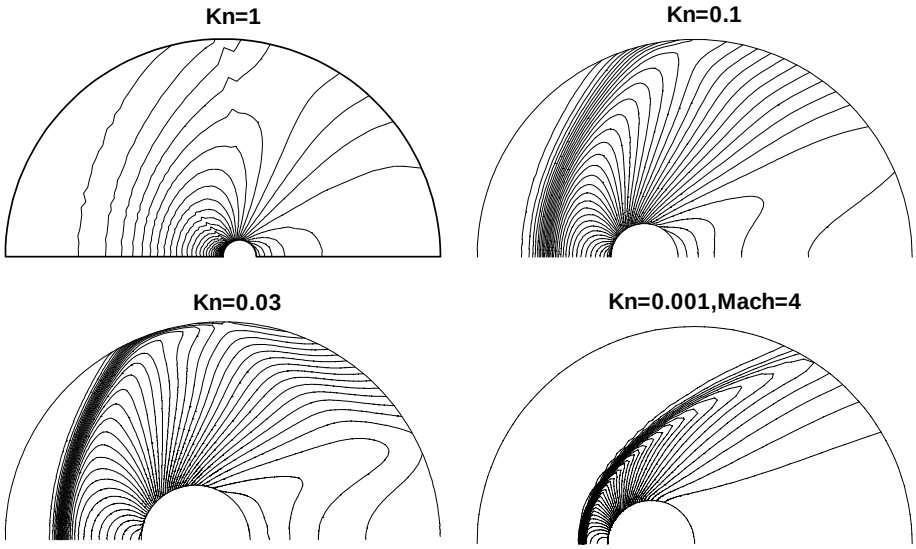

Fig. 11. Pressure contours of cylinder for supersonic flows with various Kn.

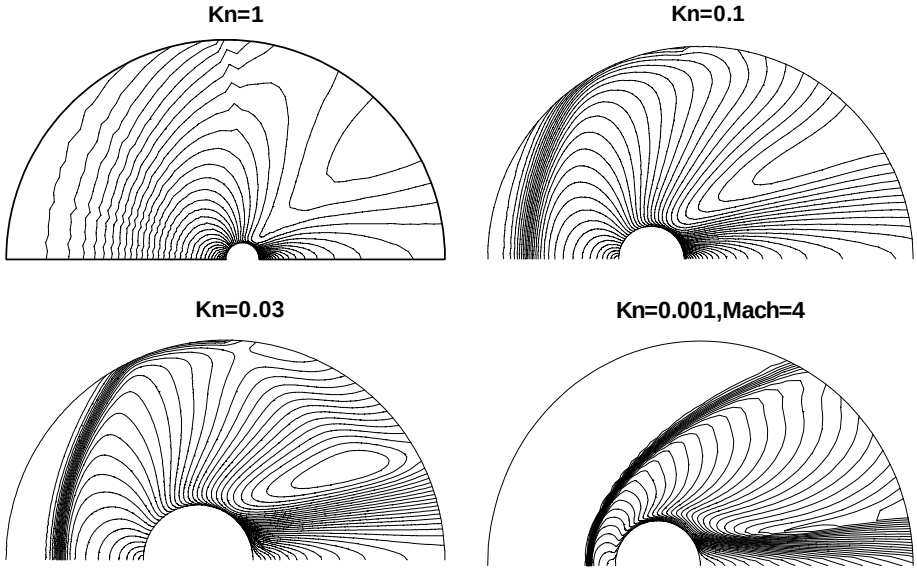

Fig. 12. Mach number contours of cylinder for supersonic flows with various Kn.

shown in Fig. 13. The flow structures including the front bow shock, the stagnation region, the recompression shock and the wake region are captured very well. An enlarged view of the recirculation zone past the circular cylinder is scored clearly in Fig. 13(e), as is only the feature of the continuum flow. For comparison purpose, the computed results from [56] using a Navier–Stokes solver (based on a high resolution finite-difference method) are also shown in Fig. 14 for the similar flow conditions ($\mathrm{Re}_D = 2996$, $M_\infty = 1.8$). By comparing the results shown in Fig. 13 to those shown in Fig. 14, it can be found that most of the flow structures are similar. The distribution of the pressure along wall surface for the state of $Kn = 0.0001$ and $M_\infty = 1.8$ is shown in Fig. 15 together with the continuum theoretic data from [57]. In Fig. 15, the horizontal coordinates denote the angle along wall surface far from the stagnation line between the free-stream direction and the outward direction normal to the wall surface, the vertical coordinates denote the non-dimensional pressure, the symbols (○) indicate the continuum theoretic solutions from [57], the symbols (●) indicate the computed results. It is shown that the computed results agree with the continuum theoretic data. The foregoing comparisons from Figs. 13–15 confirm that the present method is reliable in solving continuum gas flows.

The stagnation line profiles of density are shown in Fig. 16 together with the DSMC results from [58] for two Knudsen numbers ($Kn = 1,\ 0.3$) with the states of $M_\infty = 1.8$, $Pr = 1$, $T_\mathrm{w}/T_0 = 1$. Here, the space grid system used is 41×35, and the modified Gauss–Hermite quadrature formula with 32×16 discrete points was employed. In Fig. 16, the solid line denotes the computed $Kn = 0.3$ results, the symbols (□) denote the DSMC results of $Kn = 0.3$, the dashed line denotes the computed $Kn = 1$ results, and the symbols (△) denote the DSMC results of $Kn = 1$. In general good agreement between the present computations and DSMC solutions can be observed.

In Fig. 17, the comparisons between the calculated cylinder drag coefficients and experimental data for argon gas are given for the cases of $M_\infty = 1.96$, $Pr = 2/3$, $T_\mathrm{w}/T_0 = 0.7$, $\gamma = 5/3$, $Kn = 6,\ 0.6,\ 0.08,\ 0.01,\ 0.001$ and 0.0001. The symbols (○) denote the experimental data from [59] and the relevant continuum flow limit solution, and the symbols (●) denote the computed results. It is shown that the computed results agree with the experimental data very well.

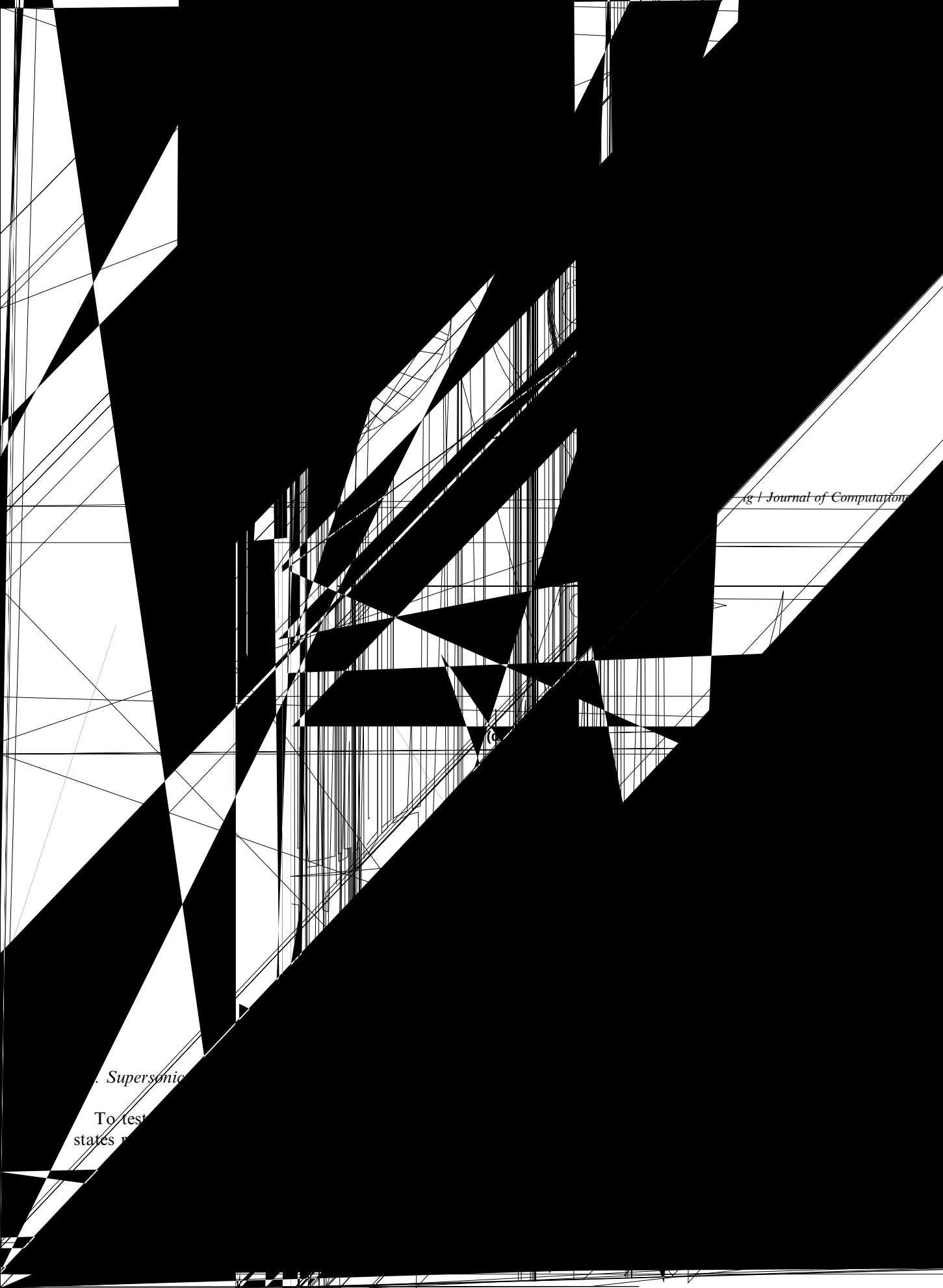

. Supersonic

To test
states r

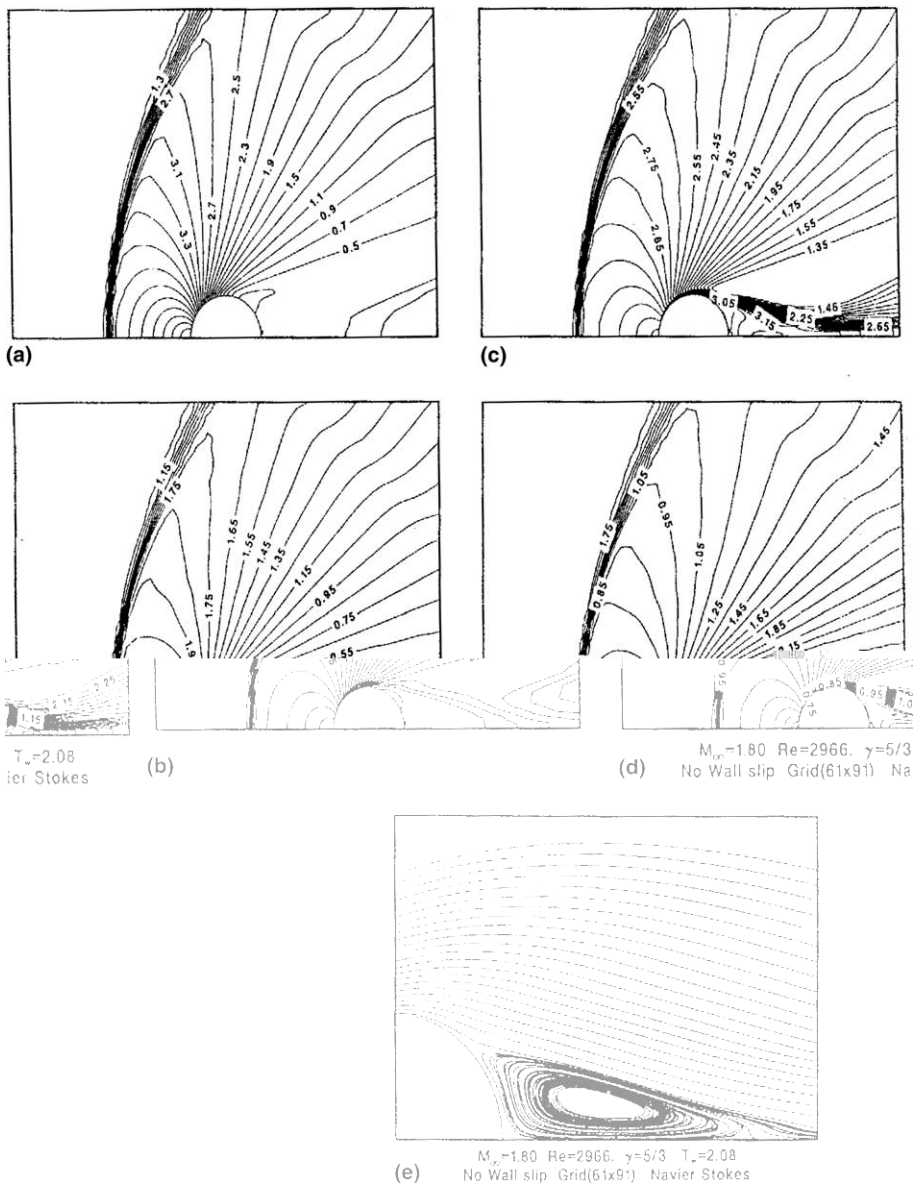

Fig. 14. Continuum Navier–Stokes solutions past cylinder for $M_\infty = 1.8$, $\mathrm{Re}_D = 2966$ from [56]. (a) Pressure; (b) density; (c) temperature; (d) Mach no.; (e) practical tracing.

sphere were simulated in a 512M microcomputer. The $31 \times 19 \times 25$ space cells of the streamwise, circumferential and surface normal directions and the modified Gauss–Hermite quadrature formula were used with $16 \times 14 \times 14$ discrete velocity grid points. In Table 1, the comparisons between the calculated sphere drag coefficients and the experimental data from [60] are shown. The computed results agree with the experimental data well. The computational results of the pressure contours in the symmetry plane are shown in Fig. 18 for the foregoing case of $Kn = 0.0126$. It is shown that the thickening of the front bow shock is the noticeable characteristics in the rarefied transition flow.

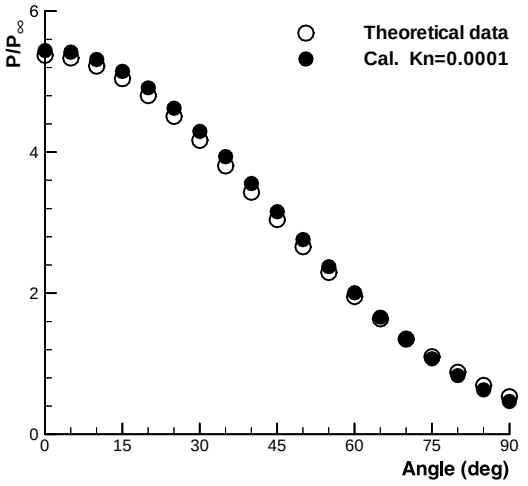

Fig. 15. Pressure distribution along surface.

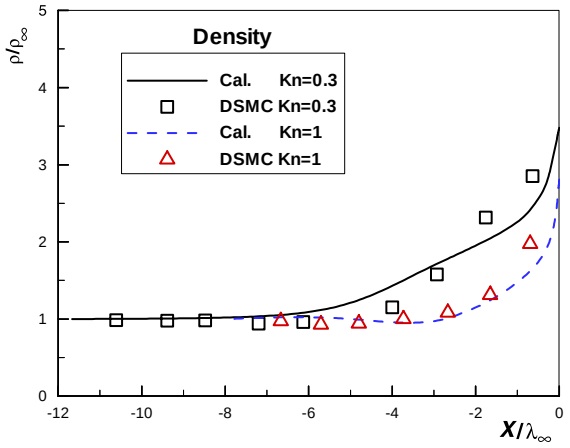

Fig. 16. Stagnation line density profiles.

6. Development of HPF parallel code for the unified algorithm

It has been made out from the computation of the three-dimensional flows that the present unified algorithm requires to use six-dimensional array to access the discrete velocity distribution functions for every points in the discrete velocity space and physical space so that a great deal of computer memory needs to be occupied in solving three-dimensional flow problems. It is impractical by using serial computers at the present time for the present algorithm to run the careful computation of three-dimensional complex problems. On the other hand, it has been shown from the study that the gas kinetic algorithm solving the velocity distribution functions in the phase space consisting of the velocity space and the physical space can be split up into two parts, one is that the discrete velocity distribution functions can be solved independently and concurrently by the numerical method described in Section 4 at every given discrete velocity points, the other is on the basis of the solved discrete velocity distribution functions that the macroscopic

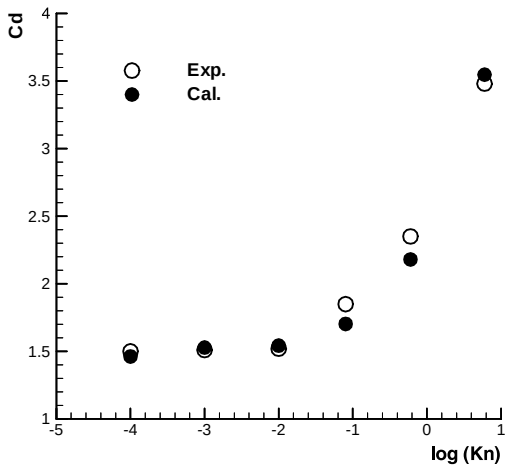

Fig. 17. Drag coefficients of cylinder.

Table 1
Drag coefficients of sphere for $M_\infty = 2$ with various Kn

Kn	Calculated[a]	Experimental[b]	Error (%)[c]
0.0126	1.7049	1.5997	6.58
0.0232	1.7467	1.6621	5.09
0.126	2.2472	2.1779	3.18
0.248	2.3771	2.3287	2.08
1.26	3.1902	3.1494	1.30

[a] The present computed results.
[b] The experimental date from [60].
[c] The relative error.

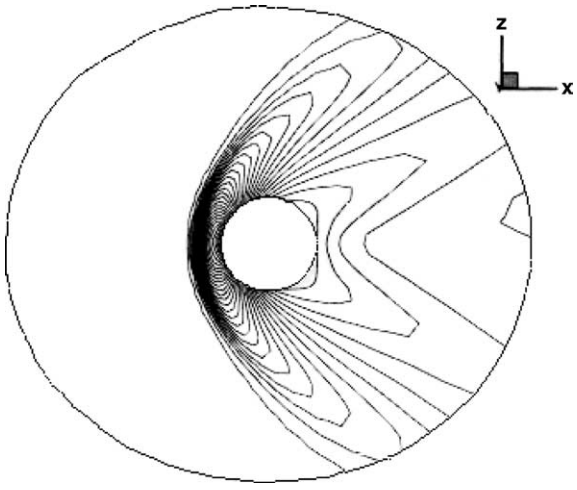

Fig. 18. Pressure contours of sphere for $Kn = 0.0126,\ M_\infty = 2$.

flow properties can be evaluated by the discrete velocity quadrature methods described in Section 3.2 at each point of the physical space. The essential and important feature of the above-mentioned computation strategy is that the calculations in the velocity space can be decoupled from those in the physical space in the gas kinetic algorithm. Consequently, the parallel processing capability of a supercomputer is quite suitable for the computation strategy in the present algorithm. The inner concurrent peculiarity of the gas kinetic numerical method makes good opportunities for computing complex flow problems. To resolve the difficulty on the vast computer memory and runtime needed by the present method in solving three-dimensional complex problems, the multi-processing strategy suitable for the gas kinetic numerical algorithm has been investigated by distributing the discrete velocity space points over processors of the supercomputer, and the parallel code software adapted to the present unified algorithm has been developed under the HPF parallel environment offered by the supercomputer from National Parallel Computing Research Center in China.

To test the performance of the HPF parallel program, the speed-up ratio and parallel efficiency are, respectively, shown in Figs. 19(a) and (b). It can be shown that the unified algorithm is quite suitable for parallel calculations, and the efficiency of concurrent calculations is found rather high.

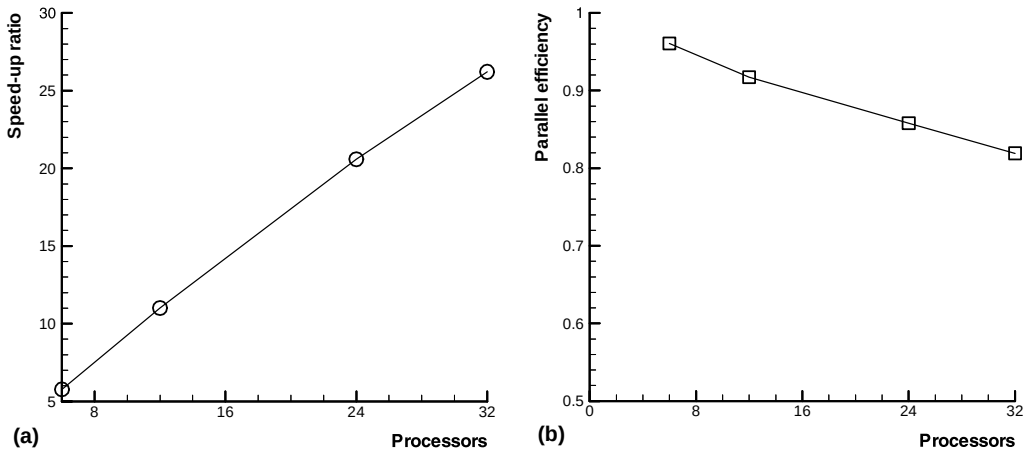

Fig. 19. (a) Sped-up ratio. (b) Parallel efficiency.

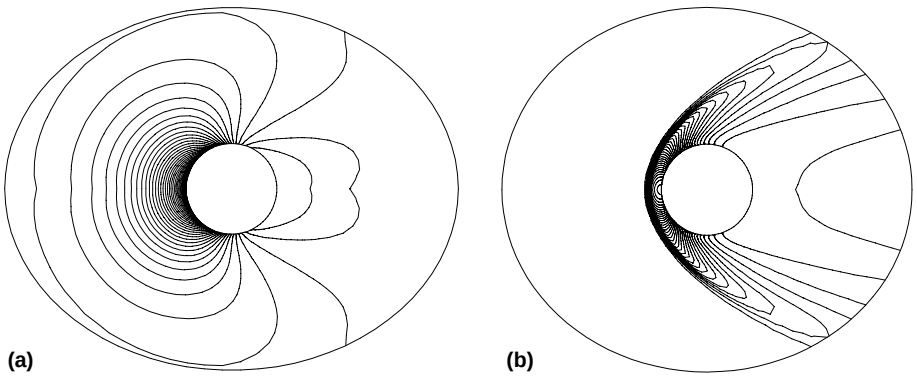

Fig. 20. Pressure contours of symmetric plane past sphere. (a) $Kn = 1$, $M_\infty = 3$; (b) $Kn = 0.005$, $M_\infty = 3$.

To verify the HPF parallel code of the unified algorithm in solving the three-dimensional flow problems from various flow regimes, the steady supersonic flows around sphere are computed under the cases of $M_\infty = 3$, $Pr = 0.72$, $T_w/T_0 = 1$, $\gamma = 1.4$, $Kn = 1$ and 0.005. The grid system used is $51 \times 41 \times 25$ in the physical space and the modified Gauss–Hermite quadrature formula was employed with $16 \times 14 \times 14$ discrete velocity ordinate points. In Fig. 20, results of concurrent calculations of the pressure contours in the symmetrical plane are presented. Fig. 20(a) describes the fully rarefied flow related to $Kn = 1$, and Fig. 20(b) describes the near continuum flow of $Kn = 0.005$ which occurs obvious bow shock and stagnation region in front of the body.

To illustrate the capability of the HPF parallel program for the flows past complex bodies, the steady supersonic rarefied flows past the spacecraft shape under various Knudsen numbers and angles of attack are computed with free stream conditions: $M_\infty = 2$, $Pr = 0.72$, $T_w/T_0 = 1$ and $\gamma = 1.4$. The space mesh of $81 \times 41 \times 19$ cells in streamwise, circumferential and surface normal directions was used. The discrete velocity grid system has $14 \times 14 \times 14$ points in (V_x, V_y, V_z) directions with the modified Gauss–Hermite quadrature formula. The parallel results of the density and Mach number contours in the symmetrical plane are, respectively, shown in Figs. 21 and 22, respected to the states of the angle of attack $\alpha = 0°$, $Kn = 5,\ 0.1$ and 0.01. The order (a), (b) and (c) in each of the figures, respectively, corresponds to results of $Kn = 5,\ 0.1$ and 0.01. Figs. 23(a)–(c), respectively, show the computed results of the density, pressure and Mach number contours in the symmetrical plane related to the aforementioned free-stream conditions with

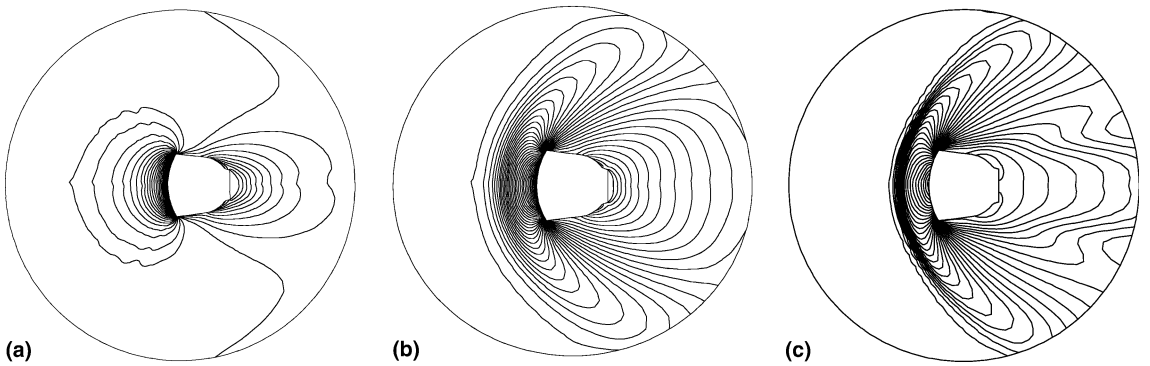

Fig. 21. Density contours in the symmetric plane past spacecraft with various Knudsen numbers. (a) $Kn = 5$, $M_\infty = 2$; (b) $Kn = 0.1$, $M_\infty = 2$; (c) $Kn = 0.01$, $M_\infty = 2$.

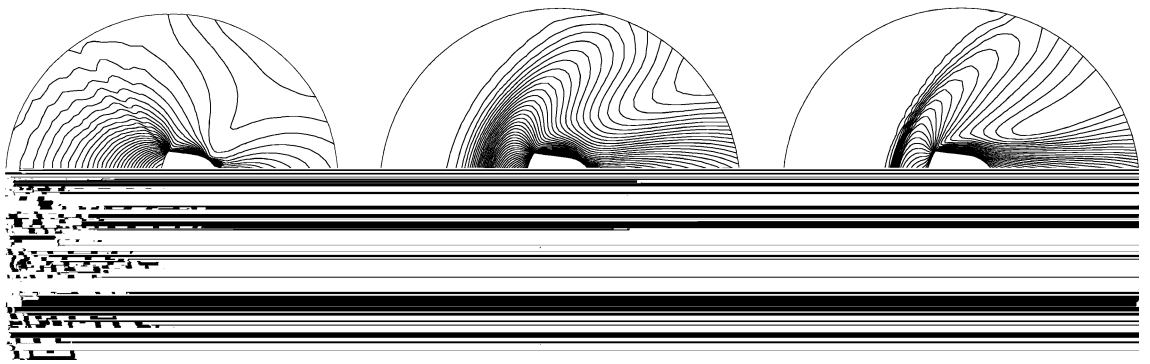

Fig. 22. Mach number contours in the symmetric plane past spacecraft with various Knudsen numbers. (a) $Kn = 5$, $M_\infty = 2$; (b) $Kn = 0.1$, $M_\infty = 2$; (c) $Kn = 0.01$, $M_\infty = 2$.

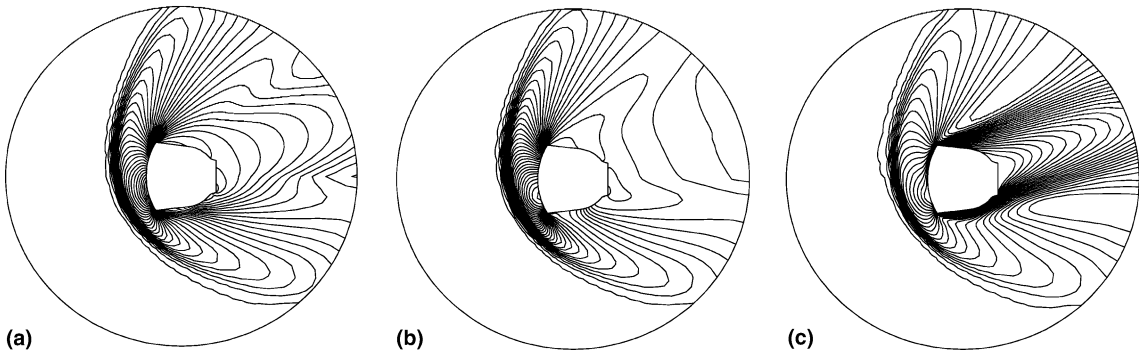

Fig. 23. Supersonic gas flow past spacecraft with $M_\infty = 2$, $Kn = 0.01$ and $\alpha = 20°$. (a) Density; (b) pressure and (c) Mach number.

$\alpha = 20°$, $Kn = 0.01$. It is shown from Figs. 21–23 that for the near continuum flow of $Kn = 0.01$, the flow structures including front bow shock, stagnation region and recompression shock are well captured, for the more rarefied flow of $Kn = 0.1$, the thickening of the front bow shock and no recompression shock in the wake flow are the noticeable differences to the flow of $Kn = 0.01$, for the near free-molecule flow of $Kn = 5$, there only exists strong disturbance around the body with no shock wave. While the Knudsen number diminishes from $Kn = 5$, $Kn = 0.1$ to $Kn = 0.01$, the gas flows past the spacecraft are gradually becoming from the near free-molecule flow, rarefied transition to the near continuum flow.

7. Concluding remarks

In this study, the Boltzmann simplified velocity distribution function equation describing microscopic molecular transport phenomena of various flow regimes is transformed into the hyperbolic conservation equations with nonlinear source terms by introducing the discrete velocity ordinate method. The discrete velocity numerical integration methods are developed for various Mach number flows to evaluate the macroscopic flow moments over the velocity space. Based on the decoupling technique on molecular movement and collision in the DSMC method, the gas kinetic unified algorithm for solving the molecular velocity distribution function has been established by the aid of the unsteady time-splitting finite difference method and the NND scheme. To test the feasibility of the present unified algorithm in solving the gas flows from rarefied transition to continuum regime, the one-dimensional shock-tube problems, the flows past two-dimensional circular cylinder and the flows around three-dimensional sphere with various Knudsen numbers are simulated in serial computers. The computational results are found in high resolution of the flow fields and good agreement with the relevant theoretical, DSMC, N–S and experimental results. The HPF parallel implementation of the unified algorithm has been developed under the data parallel environment offered by the HPF programming language. It is shown by the study that the HPF parallel algorithm has not only high parallel efficiency, but also good expansibility. To illustrate the reliability of the present HPF parallel code, the flows around sphere and the spacecraft shape with various Knudsen numbers and angles of attack are computed in the supercomputer. The concurrent calculations show that the present HPF parallel algorithm can effectively simulate the three-dimensional complex flows from various flow regimes. As the general remarks, the present method provides a considerable and efficient way that the gas dynamical problems from rarefied flow to continuum can be reliably resolved.

It has been shown from the above computations that the results of the present method are not sensitive to the grid spacing in the physical space or the velocity space if only the computing precision be satisfied, however, the finer is the grid, the better should be the precision of the results for certain at the expense of

more computing memory and time. The present method is very stable and robust without the limitation of the cell size, unlike the DSMC method which exists statistical fluctuations and requires that the grid spacing have to be less than the mean free path, in general, the computational speed of the present method seems be faster than the DSMC method in computing one- and two-dimensional problems of the rarefied flows. It has been shown from the computations that the computer time required for the present method increases as the Knudsen number decreases. In the computation of the continuum flow, as the molecular mean collision time is generally smaller than the time step determined by the stable condition of the finite difference scheme, then the computing time step given by Eq. (34) will be quite little at the magnitude of 10^{-5}, as a result, the convergent speed of the present method seems be slower than that of the Navier–Stokes solver for the continuum flow regime, especially in the computations of two- or three-dimensional continuum flows. In addition, the computations of the one- and two-dimensional flows in the present paper have been processed in the 128M microcomputers, however, the computations of three-dimensional flows have to be operated at least in 512M computers or by the parallel processing in a supercomputer.

Acknowledgements

The authors thank Prof. J.Y. Yang at Institute of Applied Mechanics, National Taiwan University, Prof. K. Xu at Hong Kong University of Science and Technology and Prof. C. Shen at Institue of Mechanics, Chinese Academy of Sciences for helpful discussion. Special thanks are due to the reviewers and editor for their many valuable comments on the original manuscript. The first author sincerely thank Prof. M.N. Macrossan at University of Queensland for his valuable suggestion and help. This work was supported by the National Nature Science Foundation of China under Grants Nos. 90205009 and 19972008, the Hypervelocity Aerodynamics Institute of CARDC in Mianyang and the National Laboratory for Computational Fluid Dynamics in Beijing.

References

[1] S. Chapmann, T.G. Cowling, The Mathematical Theory of Non-Uniform Gases, third ed., Cambridge University Press, Cambridge, UK, 1970.
[2] C. Cercignani, Kinetic Theories and the Boltzmann Equation, in: Lecture Notes in Mathematics, Springer-Verlag, Berlin/New York, 1984.
[3] G.A. Bird, Approach to translational equilibrium in a rigid sphere gas, Phys. Fluids 6 (1963) 1518.
[4] G.A. Bird, Aspects of the structure of strong shock waves, Phys. Fluids 13 (5) (1970) 1172.
[5] G.A. Bird, Direct simulation and the Boltzmann equation, Phys. Fluids 13 (11) (1970) 2676.
[6] G.A. Bird, Breakdown of translational and rotational equilibrium in gaseous expansions, AIAA J. 8 (11) (1970) 1998.
[7] G.A. Bird, Molecular Gas Dynamics and the Direct Simulation of Gas Flows, Clarendon Press, Oxford, 1994.
[8] J.N. Moss, J.M. Price, V.K. Dogra, D.B. Hash, Comparison of DSMC and experimental results for hypersonic external flow, AIAA Paper (1995) 95–2028.
[9] P.L. Bhatnagar, E.P. Gross, M. Krook, A model for collision processes in gases. I. Small amplitude processes in charged and neutral one-component systems, Phys. Rev. 94 (1954) 511.
[10] J.L. Lebowitz, H.L. Frish, E. Helfand, Nonequilibrium distribution functions in a fluid, Phys. Fluids 3 (1960) 325.
[11] T.F. Morse, Kinetic model equations in a fluid, Phys. Fluids 7 (1964) 2012.
[12] L.H. Holway Jr., New statistical models for kinetic theory, methods of construction, Phys. Fluids 9 (9) (1966) 1658.
[13] E.M. Shakov, Generalization of the krook kinetic relaxation equation, Fluid Dyn. 3 (1) (1968) 95.
[14] B.M. Segal, J.H. Ferziger, Shock-waves structure using nonlinear model Boltzmann equations, Phys. Fluids 15 (1972) 1233.
[15] T. Abe, H. Oguchi, A hierarchy kinetic model and its applications, in: J.L. Potter (Ed.), Progress in Astronautics and Aeronautics, vol. 51, Pt. II, AIAA, New York, 1977, p. 781.
[16] P. Welander, On the temperature jump in a rarefied gas, Ark. Fys. 7 (1954) 507.
[17] M.N. Kogan, On the equations of motion of a rarefied gas, Appl. Math. Mech. 22 (1958) 597.
[18] W.G. Vincenti, C.H. Kruger, Introduction to Physical Gas Dynamics, Wiley, New York, 1965.

[19] C. Cercignani, Mathematical Methods in Kinetic Theory, Revised Edition, Plenum Press, New York, 1990.
[20] D.C. Park, The Kinetic Theory of Gases with Applications in Rarefied Gas Dynamics, University of Strathclyde, Glasgow, Scotland, 1981.
[21] C. Cercignani, Rarefied Gas Dynamics: From Basic Concepts to Actual Calculations, Cambridge University Press, Cambridge, 2000.
[22] D.I. Pullin, Direct simulation methods for compressible inviscid ideal-gas flow, J. Comput. Phys. 34 (1980) 231.
[23] R.D. Reitz, One-dimensional compressible gas dynamics calculations using the Boltzmann equation, J. Comput. Phys. 42 (1981) 108.
[24] K.H. Prendergast, K. Xu, Numerical hydrodynamics from gas-kinetic theory, J. Comput. Phys. 109 (1993) 53.
[25] C. Kim, A. Jameson, A robust and accurate LED–BGK solver on unstructured adaptive meshes, J. Comput. Phys. 143 (2) (1998) 598.
[26] K. Xu, Gas-Kinetic Schemes for Unsteady Compressible Flow Simulations, 29th CFD Lecture Series 1998, vol. 3, Von Karman Institute for Fluid Dynamics, Lecture Series, Belgium, February 23–27, 1998.
[27] K. Morinishi, H. Oguchi, A computational method and its application to analyses of rarefied gas flows, in: H. Oguchi (Ed.), Proceedings of 14th International Symposium on Rarefied Gas Dynamics, Tsukubva, Japan, vol. 1, University of Tokyo Press, Tokyo, 1984, p. 149.
[28] D. Bergers, Kinetic model solution for axisymmetric flow by the method of discrete ordinates, J. Comput. Phys. 57 (1985) 285.
[29] C.H. Chung, D.R. Jeng, K.J. De Witt, T.G. Keith Jr., Numerical simulation of rarefied gas flow through a slit, J. Thermophys. 6 (1) (1992) 27.
[30] J.Y. Yang, J.C. Huang, Rarefied flow computations using nonlinear model Boltzmann equations, J. Comput. Phys. 120 (1995) 323.
[31] Z.T. Deng, G.S. Liaw, L.C. Chou, Numerical investigation of low-density nozzle flow by solving the Boltzmann model equation, 33rd Aerospace Science Meeting and Exhibit, January 9–12, 1995 (NASA-TM-110492).
[32] K. Aoki, K. Kanba, S. Takata, Numerical analysis of a supersonic rarefied gas flow past a flat plate, Phys. Fluids 9 (4) (1997) 1144.
[33] H.X. Zhang, Non-oscillatory and non-free-parameter dissipation difference scheme, Acta Aerodynamica Sinica 6 (2) (1988) 143.
[34] H.X. Zhang, F.G. Zhuang, NND schemes and their application to numerical simulation of two- and three-dimensional flows, Adv. Appl. Mech. 29 (1992) 193.
[35] B. Shizgal, A Gaussian quadrature procedure for use in the solution of the Boltzmann equation and related problems, J. Comput. Phys. 41 (1981) 309.
[36] L.K. Hua, Y. Wang, Applications of Number Theory to Approximation Analysis, Science Press, Beijing, 1978, Springer Verlag, 1981.
[37] C. Cercignani, G. Tironi, Nonlinear heat transfer between two parallel plates at large temperature ratios, in: C.L. Brundin (Ed.), Proceedings of the 5th International Symposium on Rarefied Gas Dynamics, vol. 1, Academic Press, New York, 1967, p. 441.
[38] P. Andries, B. Perthame, The ES–BGK model equation with correct Prandtl number, in: T.J. Bartel, M.A. Gallis (Eds.), Proceedings of the 22nd International Symposium on Rarefied Gas Dynamics, Sydney, Australia, vol. 585, AIP Conference Proceedings, Melville, New York, 2001, p. 30.
[39] E.M. Shakov, Kinetic model equations and numerical results, in: H. Oguchi (Ed.), Proceedings of the 14th International Symposium on Rarefied Gas Dynamics, Tsukubva, Japan, vol. 1, University of Tokyo Press, Tokyo, 1984, p. 137.
[40] A.B. Huang, D.P. Giddens, The discrete ordinate method for the linearized boundary value problems in kinetic theory of gases, in: C.L. Brundin (Ed.), Proceedings of the 5th International Symposium on Rarefied Gas Dynamics, vol. 1, Academic Press, New York, 1967, p. 481.
[41] P.C. Riedi, Thermal Physics: An Introduction to Thermodynamics Statistical Mechanics and Kinetic Theory, The Macmillan Press, London, 1976.
[42] W.E. Brittin, in: Lectures in Theoretical Physics: Kinetic theory, vol. IX C, Gordon & Breach, New York/London/Paris, 1967.
[43] A.B. Huang, D.P. Giddens, A new table for a modified (half-range) Gauss–Hermite quadrature with an evaluation of the integral, J. Math. Phys. 47 (1968) 213.
[44] Z. Kopal, Numerical Analysis, Chapman & Hall, London, 1955.
[45] Z.H. Li, Study on the unified algorithm from rarefied flow to continuum, Ph.D. thesis, China Aerodynamics Researchment and Development Center, 2001.
[46] Y. Wang, On approximation evaluation and application to integration (applications of the number theoretic method), Adv. Math. 5 (1) (1962) 1.
[47] L.K. Hua, An Optimum Seeking Theory, Science Press, Beijing, China, 1981.
[48] L.K. Hua, Y. Wang, Some Topics on Mathematical Modeling, Hunan's Education Press, Changsha, China, 1998.
[49] C.K. Chu, Kinetic-theoretic description of the formation of a shock wave, Phys. Fluids 8 (1) (1965) 12.
[50] Z.H. Li, DSMC simulation of hypersonic flow past spacecraft, in: F.G. Zhuang (Ed.), Proceedings of the ASIA Workshop on Computational Fluid Dynamics, Mianyang, China, Weicheng Press, Mianyang, 1994, p. 97.
[51] J.Y. Yang, J.C. Huang, Numerical solution of the nonlinear model Boltzmann equation, Proc. R. Soc. Lond. A 448 (1995) 55.

[52] Z.H. Li, Y.R. Xie, Technique of molecular indexing applied to the direct simulation Monte Carlo method, in: C. Shen (Ed.), Proceedings of the 20th International Symposium on Rarefied Gas Dynamics, Beijing, China, Peking University Press, Beijing, 1997, p. 205.
[53] Z.H. Li, H.X. Zhang, Study on gas kinetic algorithm for flows from rarefied transition to continuum, in: T.J. Bartel, M.A. Gallis (Eds.), Proceedings of the 22nd International Symposium on Rarefied Gas Dynamics, Sydney, Australia, AIP Conference Proceedings, vol. 585, Melville, New York, 2001, p. 628.
[54] X.G. Deng, H.X. Zhang, The extentions of NND schemes and application to viscous flow calculations, Acta Aerodyn. Sinica 12 (2) (1994) 121.
[55] H. Alsmeyer, Density profiles in argon and nitrogen shock waves measured by the absorption of an electron beam, J. Fluid. Mech. 74 (3) (1976) 497.
[56] J.Y. Yang, C.A. Hsu, High resolution, nonoscillatory schemes for unsteady compressible flows, AIAA J. 30 (1992) 1570.
[57] А.Н.Љюбимов and В.В. Русањов,ТЕЧЕНИЯ ГАЗА ОКОЛО ТУПЫХ ТЕЛ Часть II, ИЗДАТЕЛЬСТВО ⟨⟨НАУКА⟩⟩, МОСКВА, 1970, pp. 32–33.
[58] F.W. Vogenitz, G.A. Bird, J.E. Broadwell, Theoretical and experimental study of rarefied supersonic flows about several simple shapes, AIAA J. 6 (12) (1968) 2388.
[59] G.J. Maslach, S.A. Schaaf, Cylinder drag in the transition from continuum to free-molecule flow, Phys. Fluids 16 (3) (1963) 315.
[60] M. Kinslow, J.L. Potter, The Drag of Sphere in Rarefied Hypervelocity Flow, AEDC-TDR-62-205.